

A COMPUTER CODE FOR
HIGH ALTITUDE EMP

THESIS

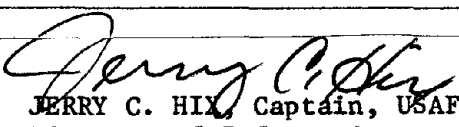
GNE/PH/74-1

Terry C. Chapman
Capt USAF

Approved for public release; distribution unlimited.

UNCLASSIFIED

SECURITY CLASSIFICATION OF THIS PAGE (When Data Entered)

REPORT DOCUMENTATION PAGE		READ INSTRUCTIONS BEFORE COMPLETING FORM
1. REPORT NUMBER GNE/PH/74-1	2. GOVT ACCESSION NO.	3. RECIPIENT'S CATALOG NUMBER <i>AD 777841</i>
4. TITLE (and Subtitle) A COMPUTER CODE FOR HIGH ALTITUDE EMP		5. TYPE OF REPORT & PERIOD COVERED THESIS
7. AUTHOR(s) Terry C. Chapman, Captain, USAF		8. CONTRACT OR GRANT NUMBER(s)
9. PERFORMING ORGANIZATION NAME AND ADDRESS AFIT/ENP Wright-Patterson AFB, OH 45433		10. PROGRAM ELEMENT, PROJECT, TASK AREA & WORK UNIT NUMBERS
11. CONTROLLING OFFICE NAME AND ADDRESS AFIT/ENP Wright-Patterson AFB, OH 45433		12. REPORT DATE January 1974
14. MONITORING AGENCY NAME & ADDRESS (if different from Controlling Office) Air Force Weapons Laboratory/EL Kirtland AFB, New Mexico 87117		13. NUMBER OF PAGES <i>82</i>
16. DISTRIBUTION STATEMENT (of this Report) Approved for public release; distribution unlimited		15. SECURITY CLASS. (of this report) UNCLASSIFIED
		15a. DECLASSIFICATION/DOWNGRADING SCHEDULE
17. DISTRIBUTION STATEMENT (of the abstract entered in Block 20, if different from Report) PRICES SUBJECT TO CHANGE		
18. SUPPLEMENTARY NOTES Approved for public release; IAW AFR 190-17.  JERRY C. HIX, Captain, USAF Director of Information		
19. KEY WORDS (Continue on reverse side if necessary and identify by block number) EMP High Altitude EMP EMP Computer Code		
Reproduced by NATIONAL TECHNICAL INFORMATION SERVICE U S Department of Commerce Springfield VA 22151		
20. ABSTRACT (Continue on reverse side if necessary and identify by block number) A relatively inexpensive computer code is developed to calculate the peak value of the electric field contained in an electromagnetic pulse generated by the gamma rays from a high altitude nuclear burst. The code is based on the Karzas and Latter theory for the production of Compton electrons and their interaction with the earth's magnetic field. The code can be used to calculate the peak value of the electric field at a target anywhere on or above ground level.		

UNCLASSIFIED

SECURITY CLASSIFICATION OF THIS PAGE(When Data Entered)

20.

resulting from a nuclear burst above 60 km altitude with a gamma yield up to 60 tons. Either the direct or the ground reflected wave can be calculated. With special care, bursts up to 1 kt of gamma yield can be used.

UNCLASSIFIED

SECURITY CLASSIFICATION OF THIS PAGE(When Data Entered)

A COMPUTER CODE FOR
HIGH ALTITUDE EMP

THESIS

Presented to the Faculty of the School of Engineering
of the Air Force Institute of Technology
Air University
in Partial Fulfillment of the
Requirements for the Degree of
Master of Science

by

Terry C. Chapman, B.S.
Capt USAF
Graduate Nuclear Engineering

January 1974

Approved for public release; distribution unlimited.

ic

Preface

It is my pleasure to recognize several people who contributed in various ways to make this work possible.

I want to thank my advisor, Maj Carl T. Case. His patience and helpful suggestions were important factors to the successful conclusion of this work. In addition, I want to point out that the theoretical portion of this work is based largely on a series of lectures he gave while teaching the Electromagnetic Waves (EE 6.30) course during the summer quarter of 1973. His unusual ability to present difficult topics in a way that is easily understood by the student was the largest and most important contribution to the success of this work.

I want to thank Dr. Charles J. Bridgman for his suggestions and helpful comments made during the early stages of the work.

I want to thank Capt Frank N. Fredrickson and Lt John R. Lillis for taking the time to discuss various problems, ideas, and solutions with me.

Last, but not least, I want to gratefully acknowledge the large contribution of my wife, Karen. She offered moral support, punched computer cards, typed drafts, and in many other ways contributed to the successful conclusion of this work.

Terry C. Chapman

Contents

Preface	ii
List of Figures	iv
Abstract	v
I. Introduction	1
II. Theory	4
Overview	4
Electron Current and Densities	4
Gamma Transport	4
Electron Currents and Densities	6
Relativistic Electron Motion	9
Transformation to Spherical Coordinates	10
Electromagnetic Fields from High Altitude	
Currents	13
Maxwell's Equations	13
Transformation to Spherical Coordinates	
and Retarded Time	14
High Frequency Approximation	17
III. Code Description	20
General Approach	20
Inputs	24
Preliminary Calculations	25
Calculation of Compton Currents and	
Conductivity	25
Integration of Field Equations	27
Outputs	27
IV. Results of Input Parameter Variation	29
V. Discussion and Recommendations	40
Limitations	40
Uses	41
Recommendations	41
Bibliography	43
Appendix A: EMP Code User's Guide	44
Appendix B: EMP Code Flow Charts	48
Appendix C: EMP Code Listing	57
Vita	73

List of Figures

<u>Figure</u>		<u>Page</u>
1.	Geometry of the Burst.	5
2.	Descriptive Flow Chart	21
3.	Target Geometry	23
4.	Output from a Typical Run.	30
5.	Plot of $E(\tau)$ at Target from a Typical Run	31
6.	Variation in the X Direction	33
7.	Variation in the Y Direction	34
8.	Variation in the Z Direction	35
9.	Variation in Height of Burst	37
10.	Variation in Gamma Yield	39

Abstract

A relatively inexpensive computer code is developed to calculate the peak value of the electric field contained in an electromagnetic pulse generated by the gamma rays from a high altitude nuclear burst. The code is based on the Karzas and Latter theory for the production of Compton electrons and their interaction with the earth's magnetic field.

The code can be used to calculate the peak value of the electric field at a target anywhere on or above ground level, resulting from a nuclear burst above 60 km altitude with a gamma yield up to 60 tons. Either the direct or the ground reflected wave can be calculated. With special care, bursts up to 1 kt of gamma yield can be used.



A COMPUTER CODE FOR HIGH ALTITUDE EMP

I. Introduction

The effects of a nuclear environment on aerospace systems is an important factor in systems analysis. During the past few years several students have worked with Professor Bridgman at the Air Force Institute of Technology (AFIT) on a computer code to determine survivability of a system with known nuclear vulnerabilities from a variable nuclear threat. The AFIT survivability code capabilities include blast, thermal, x-ray, gamma ray, and neutron effects. The high altitude EMP code presented in this report is intended to be used in conjunction with the AFIT survivability code.

The EMP (electromagnetic pulse) from a nuclear weapon is usually considered to be a radiating electromagnetic wave of short duration containing many frequencies. However, the nuclear generated EMP was not studied seriously until a considerable time after the first nuclear explosion. At present there is a significant amount of work being done to model EMP generation and effects. For example the Air Force Weapons Laboratory (AFWL) and several civilian companies under contract to the USAF are working in the field.

There are several different types of EMP with distinctions made between the mechanisms which generate them. Kinsley (Ref 1) presents a comprehensive discussion of the various types of EMP. For example, a nuclear burst on the ground produces an EMP with different characteristics

than those from a high altitude burst. Also, nuclear burst products interacting directly with a system can produce an EMP within the system or even within the circuits of the system. This report considers only the EMP generated by high altitude burst gamma rays interacting with the atmosphere.

The high altitude EMP code developed in this report is based on the theory of Karzas and Latter (Ref 2). Briefly, the theory develops a model for the interaction of Compton electrons with the geomagnetic field. The Compton electrons are produced by prompt gamma radiation from the burst in a reasonably well defined region in the atmosphere. Several simplifications are made before arriving at the final equations.

Since several of the simplifications and assumptions used are implicit in the presentation of the theory, it is appropriate to list them here. Only one group of monoenergetic unscattered gamma rays are considered to produce Compton electrons. Each gamma which interacts is assumed to produce one and only one Compton electron initially traveling precisely in the radial direction. No angular distribution of Compton electrons is allowed. All Compton electrons are assumed to have the same energy. Curvature of the Earth's magnetic field is ignored. The electromagnetic fields are not self-consistent, that is, only the geomagnetic field is considered to affect the motion of the Compton electrons. Cascading of secondary electrons and recombination of ions is ignored. The low

frequency portion of the pulse is not considered. The Earth is assumed to be flat and the finite conductivity of ground is not considered. The burst is assumed to be far from the absorption region. Only gamma ray effects are considered.

Although the final model is somewhat restricted by these assumptions and simplifications, the end result is a relatively inexpensive computer code which gives a peak value of the electric field at any target point on or above the ground, which is an upper bound on the actual peak value.

Section II of this report develops the theory and derives the equations used in the code. Section III describes the calculational procedures used in the code. Section IV presents a sample of typical results and a study of input parameter variation. Section V is a discussion of the code's limitations and uses, with recommendations for possible improvements. Appendix A is a code user's guide. Appendix B is the detailed flow charts for the entire code. And finally Appendix C is a listing of the complete code.

II. Theory

Overview

The EMP problem is a problem in classic electromagnetic theory. A solution of Maxwell's equations is a solution of the problem. In this case it is necessary to model the current and charge densities generated by the gamma rays in the absorption region to obtain the sources and conductivity needed to solve Maxwell's equations.

Expressions for the current sources and conductivity are obtained in four steps. The transport of the gammas from the burst to the absorption region is used to obtain the number density of reacting gammas. This result is used with the models for the current and charge densities to obtain preliminary expressions. Then after considering the relativistic motion of the Compton electrons, the preliminary expressions are transformed to spherical coordinates.

After presenting Maxwell's equations in a convenient form, they are transformed to spherical coordinates and retarded time. A high frequency approximation is then made to arrive at the final equations.

Electron Current and Density

Gamma Transport. Consider the geometry shown in Fig. 1. The nuclear burst occurs at the origin at time, $t = 0$. The gamma rays move to point r' in time t' and at that point and time interact to create Compton electrons. It is assumed

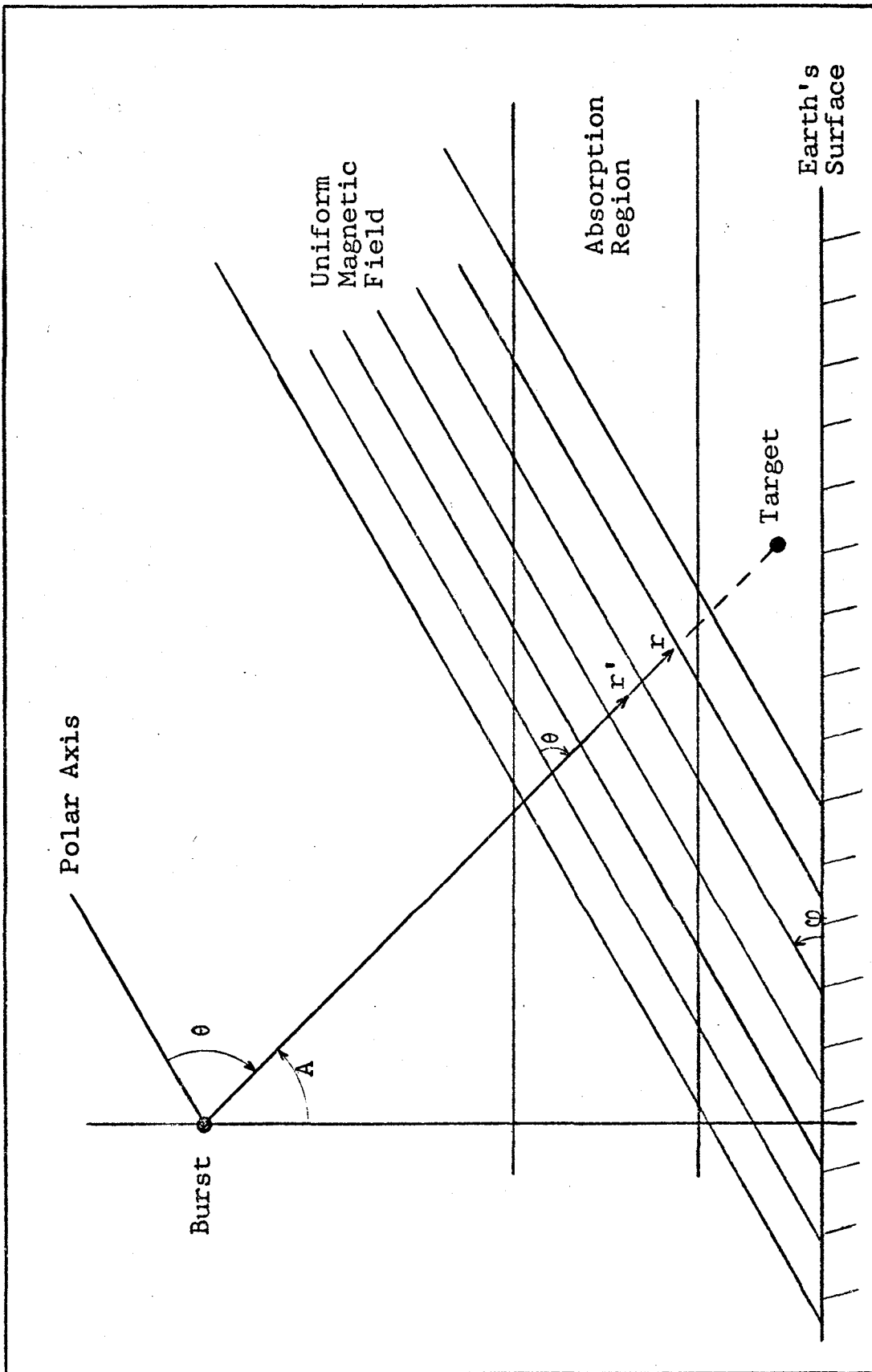


Fig. 1. Geometry of the Burst

that each gamma creates one and only one Compton electron traveling in the radial direction with the maximum Compton recoil energy.

The gamma ray emission rate can be taken as

$$\frac{dN(t)}{dt} = \frac{Y}{E} f(t) \quad (1)$$

where

$N(t)$ = number of gamma rays emitted

Y = gamma ray yield of burst

E = mean energy of the gamma rays

$f(t)$ = time dependence of the yield

and

$$\int_{-\infty}^{\infty} f(t) dt = 1 \quad (2)$$

The number density of gammas, $g(r)$, which interact at a point, r , can be taken as

$$g(r) = \frac{Y}{E} \frac{\exp \left\{ - \int_0^r \frac{dr'}{\lambda(r')} \right\}}{4\pi r^2 \lambda(r)} \quad (3)$$

where

λ = mean free path for production of Compton electrons.

Electron Currents and Densities. The rate of production of primary (Compton) electron density, n_{pri} , is

$$\frac{dn_{pri}}{dt} = g(r)f(t - r/c) \quad (4)$$

Following the Karzas-Latter approach (Ref 2) it is assumed that the electrons maintain their initial speed, V_0 , throughout their range, R, and then abruptly stop. Also, it is assumed that the secondary electrons are made at a uniform rate during the lifetime, R/V_0 , of the Compton electrons. Therefore, the rate of production of secondary electron density, n_{sec} , is

$$\frac{dn_{sec}}{dt} = \left\{ \frac{E_{pri}/33\text{ev}}{R/V_0} \right\} n_{pri} = \frac{qV_0}{R} n_{pri} \quad (5)$$

where

E_{pri} = the initial energy of the Compton electrons

R = the range of the Compton electrons in air

q = $E_{pri}/33\text{ev}$

33ev = average ionization energy per molecule for air

V_0 = the speed of the Compton electrons

R/V_0 = the lifetime of the Compton electrons

Now consider the current resulting from the Compton electrons. The differential current is the charge times the velocity times the differential density of electrons.

Hence

$$d\vec{J}^c = -e\vec{V}(t-t')g(r')f(t' - r'/c)dt' \quad (6)$$

where

$\vec{V}(t-t')$ = velocity of the Compton electrons at time t which were created at time t' .

Putting (6) into integral form gives

$$\vec{J}^c = -e \int_{t-R/V_0}^t g(r') f(t' - r'/c) \vec{V}(t-t') dt' \quad (7)$$

Now let

$$\tau' = t - t' \quad (8a)$$

$$\tau = t - (r/c) \quad (8b)$$

$$X(\tau') = X(\tau) = r - r' \quad (8c)$$

Also note that

$$(r-r') \ll r \text{ or } r' \quad (9)$$

for distant explosions (see Fig. 1). So,

$$g(r) \approx g(r') \quad (10)$$

Using Eqs (8), (9), and (10) in Eq (7) gives

$$\vec{J}^c = -eg(r) \int_0^{R/V_0} \vec{V}(\tau') f\left(\tau - \tau' + \frac{X(\tau')}{c}\right) d\tau' \quad (11)$$

Using similar arguments,

$$n_{pri} = g(r) \int_0^{R/V_0} f\left(\tau - \tau' + \frac{X(\tau')}{c}\right) d\tau' \quad (12)$$

And putting Eq (12) into Eq (5) yields

$$n_{sec} = \frac{qV_0}{R} \int_{-\infty}^{\tau} n_{pri}(\tau') d\tau'$$

$$= g(r) \frac{qV_0}{R} \int_{-\infty}^{\tau} \left[\int_0^{R/V_0} f \left(\tau' - \tau'' + \frac{x(\tau'')}{c} \right) d\tau'' \right] d\tau' \quad (13)$$

Relativistic Electron Motion. Equations (11), (12), and (13) contain $r(\tau)$ and $X(\tau)$ which are not yet defined in an easily obtained form. The equation of motion for a Compton electron is

$$\frac{d}{dt} (\vec{m}\gamma\vec{v}) = -e\vec{v}\times\vec{B}_0 \quad (14)$$

where

m = electron rest mass

$\gamma = [1 - (V/c)^2]^{-1/2}$

\vec{B}_0 = earth's magnetic field = $B_0 \hat{U}_z$

Again it is assumed that V_0 is constant throughout the electron's lifetime.

With $\omega = eB_0/m\gamma$ Eq (14) becomes

$$\frac{d}{d\tau} \vec{v}(\tau) = -\vec{v}(\tau) \times \hat{U}_z \omega \quad (15)$$

Breaking Eq (15) into its rectangular components

$$\frac{dv_x}{d\tau} = -\omega v_y \quad (16a)$$

$$\frac{dV_y}{d\tau} = \omega V_x \quad (16b)$$

$$\frac{dV_z}{d\tau} = 0 \quad (16c)$$

A solution for this set of equations is

$$V_x = V_{\perp} \cos \omega \tau \quad (17a)$$

$$V_y = V_{\perp} \sin \omega \tau \quad (17b)$$

$$V_z = V_{||} \quad (17c)$$

where V_{\perp} is the initial velocity component perpendicular to \vec{B}_0 and $V_{||}$ is the initial velocity component parallel to \vec{B}_0 and both are constants with respect to τ .

Transformation to Spherical Coordinates. It is convenient to transform the above solution to a spherical coordinate system with its origin at the burst point. The transformation from rectangular to spherical coordinates is

$$V_r = V_x \sin \theta \cos \phi + V_y \sin \theta \sin \phi + V_z \cos \theta \quad (18a)$$

$$V_{\theta} = V_x \cos \theta \cos \phi + V_y \cos \theta \sin \phi - V_z \sin \theta \quad (18b)$$

$$V_{\phi} = -V_x \sin \phi + V_y \cos \phi \quad (18c)$$

Without loss of generality the coordinates can be chosen such that \vec{V} lies in the X-Y plane, hence $\phi = 0$, and the transformation becomes

$$v_r = v_x \sin \theta + v_z \cos \theta \quad (19a)$$

$$v_\theta = v_x \cos \theta - v_z \sin \theta \quad (19b)$$

$$v_\phi = v_y \quad (19c)$$

Note that

$$v_\perp = v_0 \sin \theta \quad (20a)$$

$$v_{\parallel} = v_0 \cos \theta \quad (20b)$$

Putting Eqs (17) and (20) into Eq (19) gives

$$v_r = v_0 [\sin^2 \theta \cos \omega \tau + \cos^2 \theta] \quad (21a)$$

$$v_\theta = v_0 [\cos \theta \sin \theta \cos \omega \tau - \sin \theta \cos \theta] \quad (21b)$$

$$v_\phi = v_0 [\sin \theta \sin \omega \tau] \quad (21c)$$

Now $X(\tau)$ can be written as

$$X(\tau) = \int_0^\tau v_r d\tau = v_0 [\sin^2 \theta \frac{\sin \omega \tau}{\omega} + \tau \cos^2 \theta] \quad (22)$$

Equations (21) and (22) substituted into Eq (11) give

$$J_r^C = -eg(r)v_0 \int_0^{R/V_0} f(T) [\cos^2 \theta + \sin^2 \theta \cos \omega \tau'] d\tau' \quad (23)$$

$$J_\theta^C = -eg(r)v_0 \int_0^{R/V_0} f(T) [\sin \theta \cos \theta (\cos \omega \tau' - 1)] d\tau' \quad (24)$$

$$J_\phi^C = -eg(r)v_0 \int_0^{R/V_0} f(T) [\sin \theta \sin \omega \tau'] d\tau' \quad (25)$$

where

$$T = \tau - (1 - \beta \cos^2 \theta) \tau' + \beta \sin^2 \theta \frac{\sin \omega \tau'}{\omega} \quad (26a)$$

with

$$\beta = V_0/c \quad (26b)$$

Equations (23), (24), (25), and (26) provide the Compton currents within the absorption region in a form which can be used in the final field equations. In addition to the Compton currents, an expression for the conductivity within the absorption region is needed.

Equations (21) and (22) substituted into Eq (13) give

$$n_{sec}(\tau) = \frac{qV_0}{R} g(r) \int_{-\infty}^{\tau} \left[\int_0^{R/V_0} f(T') d\tau'' \right] d\tau' \quad (27)$$

where

$$T' = \tau' - (1 - \beta \cos^2 \theta) \tau'' + \beta \sin^2 \theta \frac{\sin \omega \tau''}{\omega} \quad (28)$$

Consider the equation of motion for secondary electrons. Neglecting the $\vec{V} \times \vec{B}_0$ term, which is small compared to the other terms (Ref 2) it is

$$m \frac{d\vec{V}}{dt} = -e\vec{E} - m\vec{V}v_c \quad (29)$$

where

v_c = electron collision frequency.

These secondary electrons have velocities in the thermal region and are assumed to reach their maximum velocity instantly. In this case, Eq (29) becomes

$$\vec{V} = \frac{-e}{mv_c} \vec{E} \quad (30)$$

The current source from the secondary electrons is

$$\vec{j}^{\text{sec}} = -e\vec{V}(\tau)n_{\text{sec}}(\tau) = \frac{n_{\text{sec}}(\tau)}{mv_c} e^2 \vec{E} \quad (31)$$

or in terms of conductivity

$$\vec{j}^{\text{sec}} = \sigma(\tau)\vec{E} \quad (32)$$

where

$$\sigma(\tau) = \frac{n_{\text{sec}}(\tau)}{mv_c} e^2 \quad (33)$$

Equations (32) and (33) provide the needed expressions for the conductivity.

Electromagnetic Fields from High Altitude Currents

Maxwell's Equations. Now that the Compton currents and the conductivity due to secondary electrons have been obtained, consider the field equations.

Maxwell's equations are

$$\vec{\nabla} \times \vec{E} = - \frac{\partial \vec{B}}{\partial t} \quad (34a)$$

$$\vec{\nabla} \times \vec{B} = \mu_0 \vec{J} + \frac{1}{c^2} \frac{\partial \vec{E}}{\partial t} \quad (34b)$$

$$\vec{\nabla} \cdot \vec{E} = \frac{q_v}{\epsilon_0} \quad (34c)$$

$$\vec{\nabla} \cdot \vec{B} = 0 \quad (34d)$$

where

\vec{J} = total current density

q_v = total charge density

Continuity of charge requires

$$\frac{\partial q_v}{\partial t} + \vec{\nabla} \cdot \vec{J} = 0 \quad (35)$$

It is convenient to combine the above equations into equations containing only \vec{E} in one and only \vec{B} in the other.

Doing so gives

$$\left(\nabla^2 - \frac{1}{c^2} \frac{\partial^2}{\partial t^2} \right) \vec{E} = \mu_0 \frac{\partial \vec{J}}{\partial t} + \frac{1}{\epsilon_0} \vec{\nabla} q_v \quad (36)$$

$$\left(\nabla^2 - \frac{1}{c^2} \frac{\partial^2}{\partial t^2} \right) \vec{B} = -\mu_0 \vec{\nabla} \times \vec{J} \quad (37)$$

Transformation to Spherical Coordinates and Retarded Time. Equations (36) and (37) will now be transformed to spherical coordinates and retarded time. Consider the transformation

$$\tau = t - r/c \quad (38a)$$

$$r' = r \quad (38b)$$

$$\theta' = \theta \quad (38c)$$

$$\phi' = \phi \quad (38d)$$

This is a spherical coordinate system where time is measured at each radial point in terms of the arrival of the bomb gamma rays at that point.

Using Eq (38) it is easily shown that

$$\frac{\partial}{\partial t} = \frac{\partial}{\partial \tau} \quad (39)$$

$$\frac{\partial}{\partial r} = \frac{\partial}{\partial r'} - \frac{1}{c} \frac{\partial}{\partial \tau} \quad (40)$$

$$\frac{\partial}{\partial \theta} = \frac{\partial}{\partial \theta'} \quad (41)$$

$$\frac{\partial}{\partial \phi} = \frac{\partial}{\partial \phi'} \quad (42)$$

Thus the operator

$$\frac{\partial}{\partial t}$$

transforms to

$$\frac{\partial}{\partial \tau}$$

and the operator

$$\vec{\nabla}$$

transforms to

$$\vec{\nabla} - \hat{U}_r \frac{1}{c} \frac{\partial}{\partial \tau}$$

Similarly, the operator

$$\nabla^2 - \frac{1}{c^2} \frac{\partial^2}{\partial t^2}$$

transforms to

$$\nabla^2 - \frac{2}{c} \frac{\partial}{\partial \tau} \frac{1}{r} \frac{\partial}{\partial r} r$$

Equation (36) now becomes

$$\left[\nabla^2 - \frac{2}{c} \frac{1}{r} \frac{\partial}{\partial \tau} \frac{\partial}{\partial r} r \right] \vec{E} = \mu_0 \frac{\partial \vec{J}}{\partial \tau} + \frac{1}{\epsilon_0} \vec{\nabla} q_v - \hat{U}_r \frac{1}{c} \frac{\partial q_v}{\partial \tau} \quad (43)$$

and Eq (35) becomes

$$\frac{\partial q_v}{\partial \tau} = -\vec{\nabla} \cdot \vec{J} + \hat{U}_r \frac{1}{c} \frac{\partial}{\partial \tau} \cdot \vec{J} = -\vec{\nabla} \cdot \vec{J} + \frac{1}{c} \frac{\partial J_r}{\partial \tau} \quad (44)$$

Using Eq (44) in Eq (43) and rearranging gives

$$\begin{aligned} -\nabla^2 \vec{E} + \hat{U}_r \frac{1}{c \epsilon_0} \vec{\nabla} \cdot \vec{J} + \frac{1}{\epsilon_0} \vec{\nabla} q_v \\ + \frac{\partial}{\partial \tau} \left[\frac{2}{c} \frac{1}{r} \frac{\partial}{\partial \tau} (r \vec{E}) + \mu_0 (\vec{J} - \hat{U}_r \vec{J}_r) \right] = 0 \end{aligned} \quad (45)$$

Similarly, Eq (37) becomes

$$\begin{aligned} -\nabla^2 \vec{B} + \mu_0 \vec{\nabla} \times \vec{J} + \frac{\partial}{\partial \tau} \left[\frac{2}{rc} \frac{\partial}{\partial r} (r \vec{B}) \right] \\ + \frac{\partial}{\partial \tau} \left[\frac{\mu_0}{c} (\hat{U}_\phi J_\phi - \hat{U}_\theta J_\theta) \right] = 0 \end{aligned} \quad (46)$$

High Frequency Approximation. Again, following the Karzas-Latter model, note that the variation of currents with distance is slow compared to variations with time and that the fields resulting from the transverse currents are rapidly varying in character, as are the currents themselves. Therefore, only the $\partial/\partial\tau$ terms are kept in the transverse field equations. Since the radial components do not propagate outside of the absorption region, they are not considered further in this report.

The transverse equations become

$$\frac{\partial}{\partial \tau} \left[\frac{2}{c} \frac{1}{r} \frac{\partial}{\partial r} (r E_\theta) + \mu_0 J_\theta \right] = 0 \quad (47)$$

$$\frac{\partial}{\partial \tau} \left[\frac{2}{c} \frac{1}{r} \frac{\partial}{\partial r} (r E_\phi) + \mu_0 J_\phi \right] = 0 \quad (48)$$

$$\frac{\partial}{\partial \tau} \left[\frac{2}{c} \frac{1}{r} \frac{\partial}{\partial r} (r B_\theta) - \frac{\mu_0}{c} J_\phi \right] = 0 \quad (49)$$

$$\frac{\partial}{\partial \tau} \left[\frac{2}{c} \frac{1}{r} \frac{\partial}{\partial r} (r B_\phi) + \frac{\mu_0}{c} J_\theta \right] = 0 \quad (50)$$

These equations are called the Karzas-Latter high frequency approximation for the EMP fields, and they are useful in the range $0 < \tau < 100$ shakes.

Integration with respect to time yields

$$\frac{2}{c} \frac{1}{r} \frac{\partial}{\partial r} (rE_\theta) + \mu_0 J_\theta = 0 \quad (51)$$

$$\frac{2}{c} \frac{1}{r} \frac{\partial}{\partial r} (rE_\phi) + \mu_0 J_\phi = 0 \quad (52)$$

$$\frac{2}{c} \frac{1}{r} \frac{\partial}{\partial r} (rB_\theta) - \frac{\mu_0}{c} J_\phi = 0 \quad (53)$$

$$\frac{2}{c} \frac{1}{r} \frac{\partial}{\partial r} (rB_\phi) + \frac{\mu_0}{c} J_\theta = 0 \quad (54)$$

Recall that the total current density is

$$\vec{J} = \vec{J}^{\text{pri}} + \vec{J}^{\text{sec}} = \vec{J}^c + \sigma(\tau) \vec{E} \quad (55)$$

so Eqs (51) and (52) become

$$\frac{2}{c} \frac{1}{r} \frac{\partial}{\partial r} (rE_\theta) + \mu_0 J_\theta^c + \mu_0 \sigma(\tau) E_\theta = 0 \quad (56)$$

$$\frac{2}{c} \frac{1}{r} \frac{\partial}{\partial r} (rE_\phi) + \mu_0 J_\phi^c + \mu_0 \sigma(\tau) E_\phi = 0 \quad (57)$$

With the aid of a computer, it is now possible to obtain numerical solutions for the above equations which will yield a slightly high estimate of the peak value of the EMP pulse resulting from a high altitude burst.

Below the absorption region the Compton currents and the conductivity are zero. In this case, Eqs (56) and (57) have the following solutions:

$$E_\theta = C_1/r \quad (58)$$

$$E_\phi = C_2/r \quad (59)$$

where C_1 and C_2 are determined by the values of E_θ , E_ϕ , and r at the bottom of the absorption region.

III. Code Description

General Approach

Equations (56), (57), (58), and (59) were chosen as the simplest ones to solve numerically. Of course, Eqs (24), (25), (27), and (33) are used to obtain the Compton currents and conductivity needed to solve Eqs (56) and (57).

The B - field equations are not solved since

$$E = cB \quad (60)$$

can be used to obtain B once E is found. This relationship is based on the assumption that the EMP pulse is a spherical wave propagating in free space, below the absorption region.

The function used for the time dependence of the weapon yield is the one recommended by Pomranning (Ref 3).

$$f(\tau) = (1/N) \frac{(\alpha+\beta) \exp (\tau-\tau_0)}{\beta + \alpha \exp [(\alpha+\beta)(\tau-\tau_0)]} \quad (61)$$

where N is chosen such that

$$\int_0^{\infty} f(\tau) d\tau = 1 \quad (62)$$

and $\alpha > \beta$.

This function rises like $e^{\alpha\tau}$ for small τ , falls like $e^{-\beta\tau}$ for large τ , and has a single maximum at τ_0 .

Figure 2 presents a flow chart which is descriptive of the approach taken solving the equations. The top of the absorption region is assumed to be at 50 km altitude and the bottom of the absorption region is assumed to be

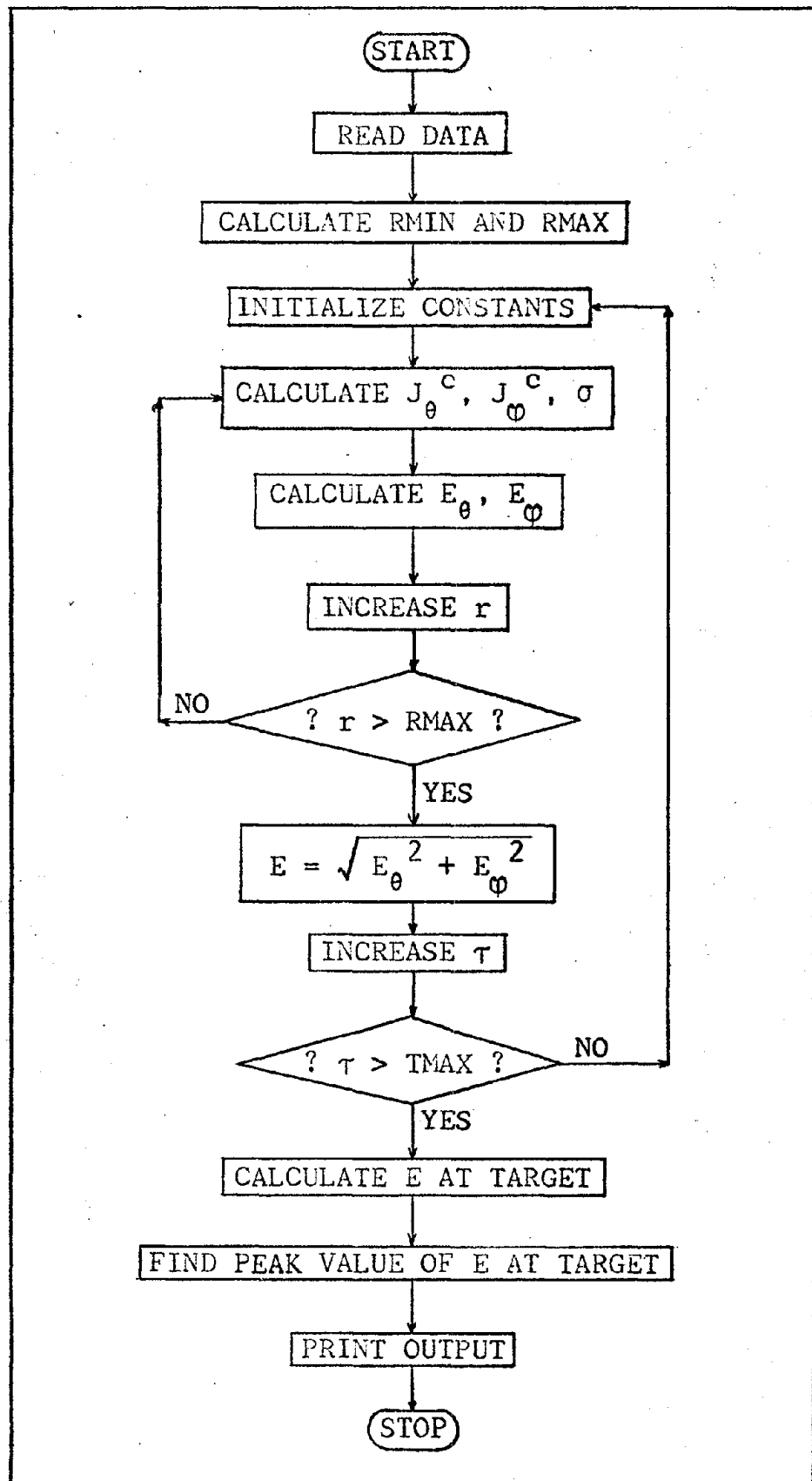


Fig. 2. Descriptive Flow Chart

at 20 km altitude. Calculations by Latter and LeLevier (Ref 4) indicate that 20 km to 50 km is the altitude where most of the prompt gamma ray energy is deposited.

Figure 3 depicts the target geometry. The value for RMIN is determined by the intersection of the line of sight with the 50 km altitude. The value for RMAX is determined by the intersection of the line of sight with the 20 km altitude. If the target is in the absorption region the target altitude determines RMAX for the direct wave calculation. These two values of r are the limits on the mesh in the r direction. The line of sight is divided into the desired number of steps along r for the integration on r in the absorption region.

The retarded time direction of the mesh is divided into 0.1 shake steps up to 10 shakes and then 1.0 shake steps on up to 100 shakes. Calculation can be stopped at any desired TMAX from 10 to 100 shakes, which is the upper limit of the usefulness of the high frequency approximation.

If the ground reflected wave is to be calculated, the mirror image of the target, below ground, is used to find the line of sight from the burst to the target.
(Refer to Fig. 3.)

At $r = RMIN$ all of the fields are assumed to be zero. For each τ , equations (57) and (58) are integrated over r from RMIN to RMAX and the value of E at the bottom of the absorption region is stored. At each step in r , equations (24), (25), and (27) are numerically integrated. Then

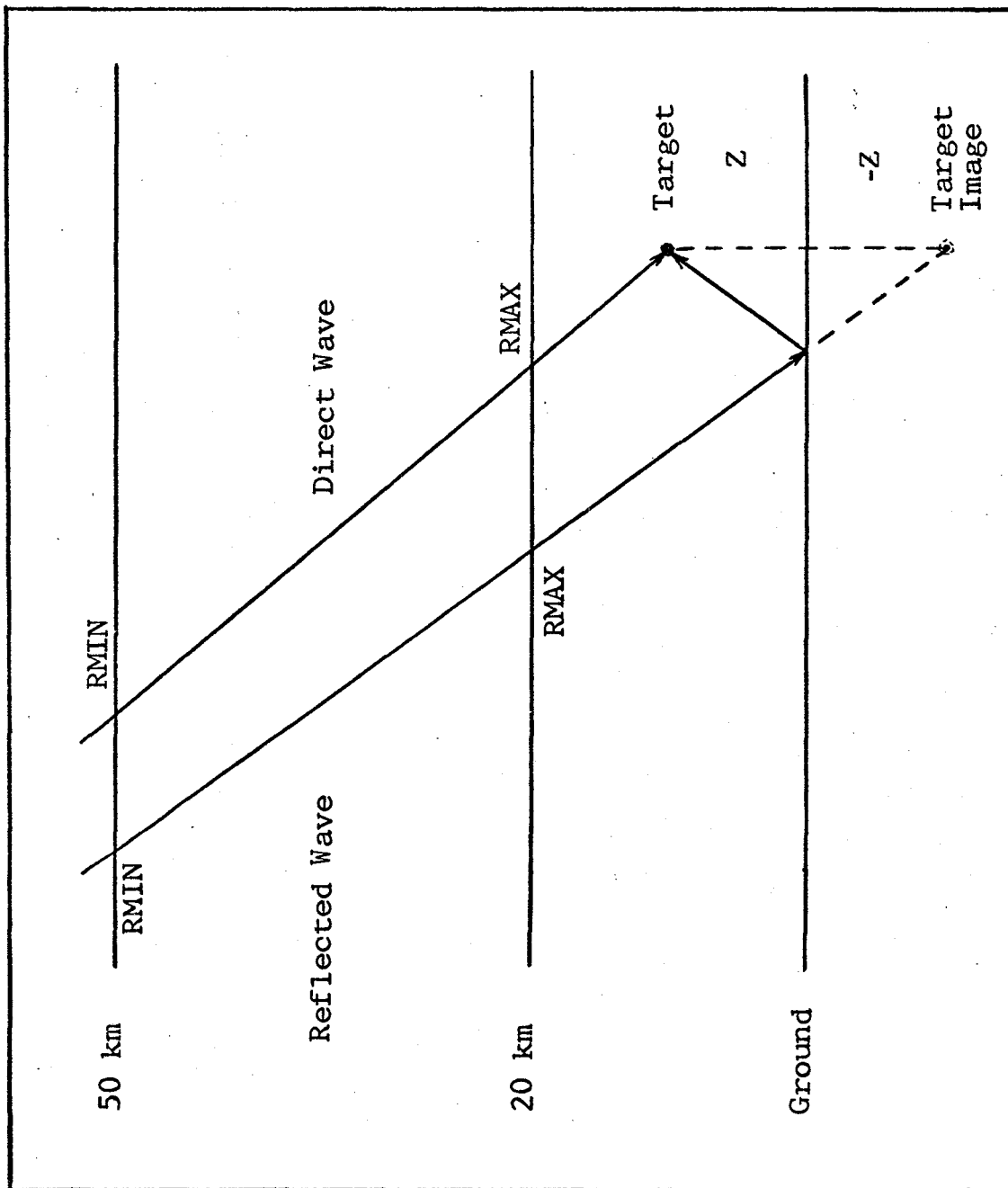


Fig. 3. Target Geometry

equations (58) and (59) are combined into

$$E = \frac{(R_{MAX})(E_{RMAX})}{r_{target}} \quad (63)$$

to find E at the target.

The E array is then searched to find the peak value before printing out the results.

Inputs

The code uses a right handed Cartesian coordinate system with the ground in the X-Y plane, the \hat{B}_0 vector in the Y-Z plane, and \hat{j} pointing towards the equator. For example, in the northern hemisphere, \hat{i} is magnetic west, \hat{j} is magnetic south, and \hat{k} is altitude. The origin of the coordinate system is always at ground zero, directly below the burst. Note that this coordinate system is not the same as the Cartesian systems used earlier.

Referring to the above coordinate system the target coordinates, (X,Y,Z), are read in using units of meters. If the reflected wave is to be calculated the altitude is read in as a negative number, (X,Y,-Z).

The height of the burst is read in using units of kilometers. The gamma yield of the burst is read in using units of kilotons.

The magnitude of the Earth's magnetic field is read in using units of webers per square meter. The dip angle (ϕ in Fig. 1) of the magnetic field is read in using units of degrees.

NDELR, the desired number of steps to be used in the integration over r in the absorption region, is read in as any integer in the closed interval [50, 500].

TMAX, the retarded time where calculations are to be stopped, is read in, using units of shakes, as any integer in the closed interval [10, 100].

Preliminary Calculations

Before starting the numerical integrations, the code performs several preliminary calculations. The input data is converted to MKS units. The reflected wave is used whenever Z is greater than 49 km or less than 0. The target coordinates are transformed to a spherical coordinate system with the burst at the origin and the polar axis parallel to \vec{B}_0 . The line of sight intersections with the absorption region are determined. And finally, the constant angles required by the code, θ and A , (see Fig. 1) are calculated.

Calculation of Compton Currents and Conductivity

The two Compton currents, J_θ^C and J_ϕ^C are calculated at each r , τ mesh point by numerically integrating equations (24) and (25). The step size used is 0.1 times the Compton lifetime, R/V_0 . The integration itself is done using the 4th order Runge-Kutta method (Ref 5). It should be noted that both the mean free path for Compton interaction and the Compton lifetime are exponentially scaled from sea

level values using a 7 km scale height. However, the Compton lifetime is not allowed to be greater than 100 shakes, since this is the maximum time of interest.

Monoenergetic gammas of energy 1.5 Mev are assumed. The most energetic Compton electrons resulting from 1.5 Mev gammas have a speed of $2.88 (10)^8$ m/sec. Therefore $v_0 = 2.88 (10)^8$ m/sec.

Since the integration on τ'' in equation (27) is also over the Compton lifetime, this integration is carried out simultaneously with the Compton current integrations. Again, the 4th order Runge-Kutta method is used. It is broken into two parts, one for $-\infty < \tau' < 0$ and the other for $0 < \tau' < \tau$. In this case, $-\infty$ is defined to be the time when the first gamma ray reached the top of the absorption region, since no secondaries can be produced before that time.

The integration on τ' in equations (27) is also broken into two parts, one for $-\infty < \tau' < 0$ and the other for $0 < \tau' < \tau$. In the first case, integration is started at $\tau' = 0$ and proceeds to $\tau' = -(r-RMIN)/v_0$ in steps of $\Delta\tau' = -\Delta r/v_0$. In the second case, integration is started at $\tau' = 0$ and proceeds to $\tau' = \tau$ in steps of $\Delta\tau' = \Delta\tau$. In both cases, simple step integration is used. That is

$$\int f(\tau') d\tau' = \sum_{\text{all } i} (\Delta\tau'_i) [f(\tau'_i)] \quad (64)$$

The integration over τ' is carried out parallel to the integration of (56) and (57) over r (using space as a pseudo retarded time) and simultaneously with the increase in τ as the space integrations are repeated for each new τ .

This rather involved approach to solving equation (27) is necessary to save running time. A direct approach, with separate integrations, would at least triple or quadruple the total running time required for execution of the code.

Integration of the Field Equations

For each τ , equations (56) and (57) are integrated from $r = RMIN$ to $r = RMAX$ in steps of $\Delta r = (RMAX-RMIN)/NDELR$ using the 4th order Runge-Kutta method. Then the magnitude of E is found from the two components and the result is stored in the E array. τ is increased by $\Delta\tau$ and the whole process is repeated until τ reaches $TMAX$.

On completion of the iterations, each member of the E array is multiplied by $RMAX/r_{target}$ (equation 62). Then the E array is searched to find the peak value.

Outputs

There are several output options available in the code. The basic output is:

1. Gamma yield and altitude of burst.
2. Target coordinates from ground zero.
3. Distance from burst to target.
4. A message indicating whether the direct or the reflected wave is being calculated.

5. The time period covered by the calculation.
6. The time when the peak value occurred.
7. The peak value of E at the target.
8. The τ and E arrays.

In addition, a linear and a log-log plot of $E(\tau)$ can be obtained. Also, a listing of the values of E at the bottom of the absorption region for each τ can be obtained. Either or both of these two options can be added to the basic output.

IV. Results and Input Parameter Variation

The output from a typical run is shown in Fig. 4.
 The $E(\tau)$ calculated during the run is shown in Fig. 5.
 The input data for this run was:

$$X = 0 \text{ meters} \quad (65a)$$

$$Y = 0 \text{ meters} \quad (65b)$$

$$Z = 0 \text{ meters} \quad (65c)$$

$$HOB = 100 \text{ km} \quad (65d)$$

$$Y_Y = .001 \text{ kt} \quad (65e)$$

$$B_0 = 2(10)^{-5} \text{ wb/m}^2 \quad (65f)$$

$$\text{Dip Angle} = 20^\circ \quad (65g)$$

$$NDELR = 50 \quad (65h)$$

$$TMAX = 20 \text{ shakes} \quad (65i)$$

The CDC 6600 Computer required 191 sec and 33000_8 words of central memory to execute this run.

The peak value of E , 6400 V/m, obtained in this run compares favorably with Karzas-Latter's order of magnitude estimate of 10^4 V/m (Ref 2) from similar input data.

In order to gain a better knowledge of the operating capabilities of the code, the effect of varying input parameters one at a time was studied. The basic set of parameters used was:

THE BURST WITH GAMMA YIELD OF 1.000E-03 KILOTONS
IS AT AN ALTITUDE OF 1.000E+02 KILOMETERS.

THE TARGET IS AT COORDINATES
WHICH IS 1.000E+05 METERS FROM THE BURST

0.
0.

DIRECT WAVE IS BEING CALCULATED

ITERATION TERMINATED AFTER 20.0 SHAKES

PEAK OCCURRED AT 2.1 SHAKES

* * * * *
* PEAK FIELD AT TARGET IS 6.448E+03 VOLTS/METER
* * * * *

Fig. 4. Output from a Typical Run

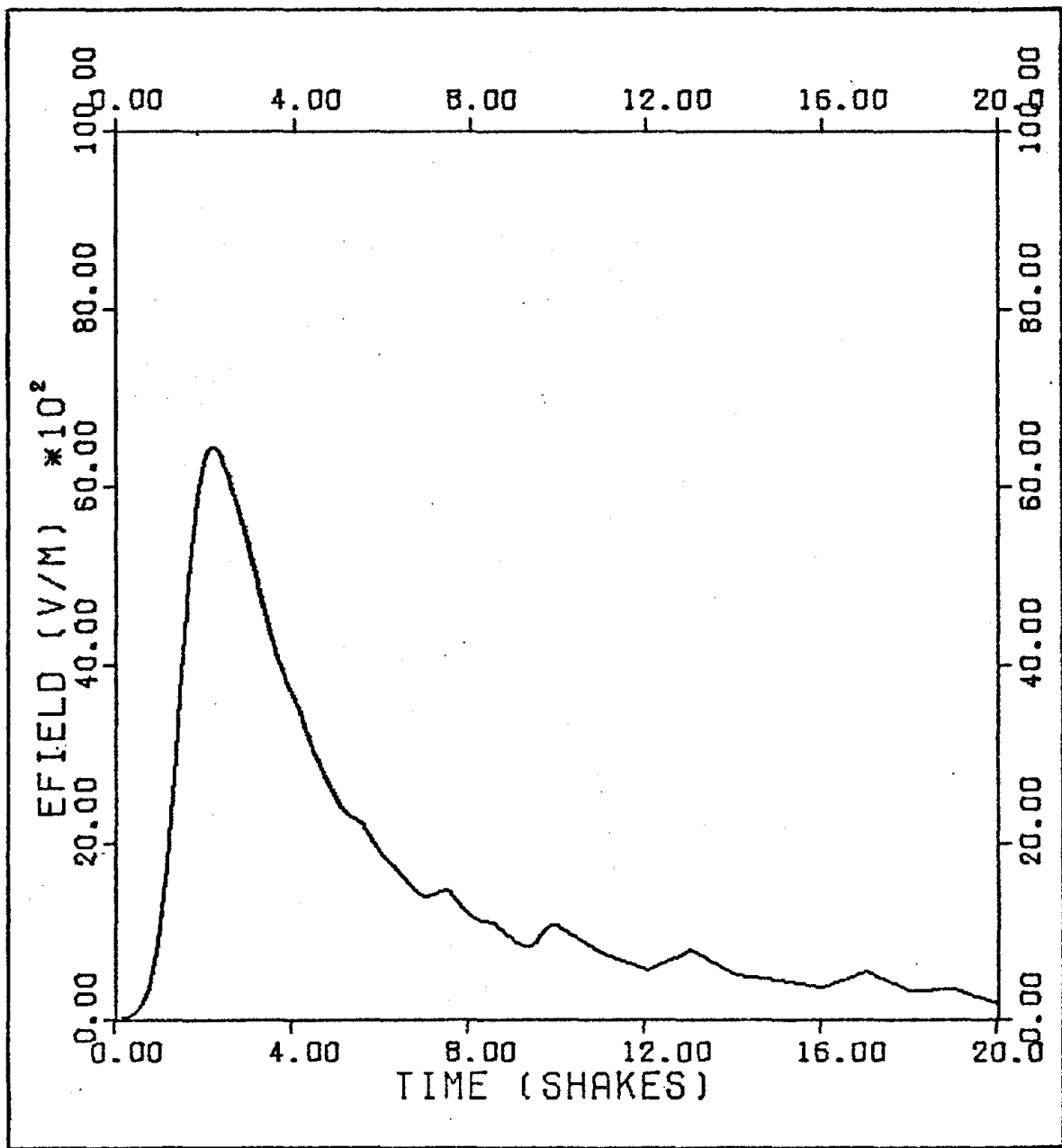


Fig. 5. Plot of $E(\tau)$ at target from a typical run

X = 0 meters	(66a)
Y = 0 meters	(66b)
Z = 0 meters	(66c)
HOB = 100 km	(66d)
$V_Y = .001 \text{ kt}$	(66e)

Each of the above parameters was systematically varied while holding the others constant. The other inputs were held constant at the values shown in equations (65).

The results of the variation in X are shown in Fig. 6. Since the X axis is perpendicular to the magnetic field the symmetry about $X = 0$ is expected. The decrease in peak value of E for increasing distance from ground zero is due to the increasing distance from the burst.

The results of the variation in Y are shown in Fig. 7. Here the peak values of E depend on the angle between \vec{r} and \vec{B}_0 , θ . When $\theta = 180^\circ$ ($A = -70^\circ$ and $Y = -275 \text{ km}$) the peak E drops to zero. The maximum peak E is skewed toward $A = 20^\circ$ ($\theta = 90^\circ$ and $Y = 36 \text{ km}$). The maximum is not exactly at $A = 20^\circ$ because of the increased distance from the burst. These characteristics are expected since an electron moving perpendicular to the magnetic field would feel the strongest acceleration from it while an electron moving parallel to the magnetic field would feel no acceleration at all.

The results of variation in Z are shown in Fig. 8. In this case, both the direct and the reflected waves were calculated at each point below the top of the absorption

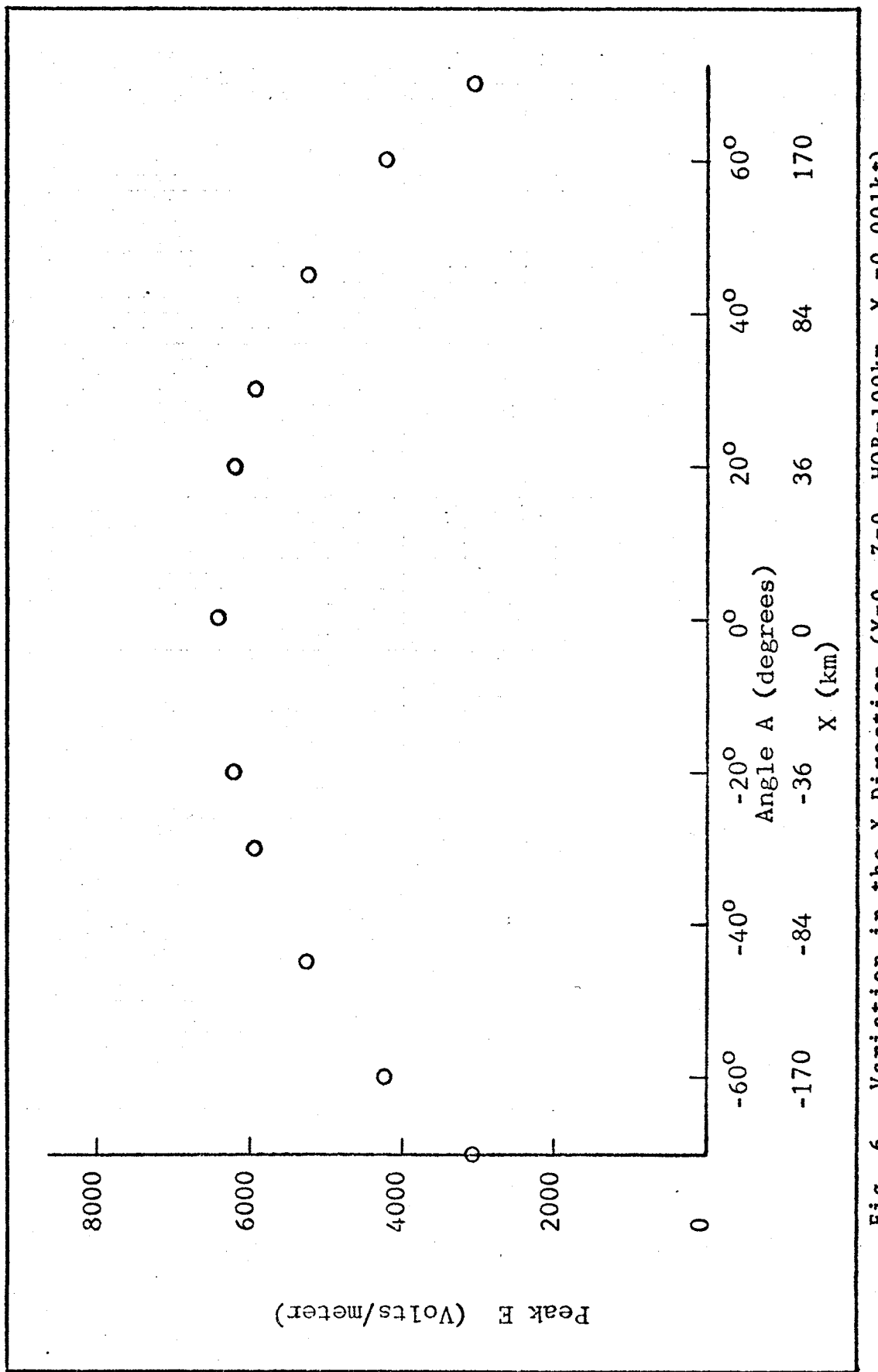


Fig. 6. Variation in the X Direction ($Y=0$, $Z=0$, $HOB=100\text{km}$, $\Upsilon_\gamma=0.001\text{kt}$)

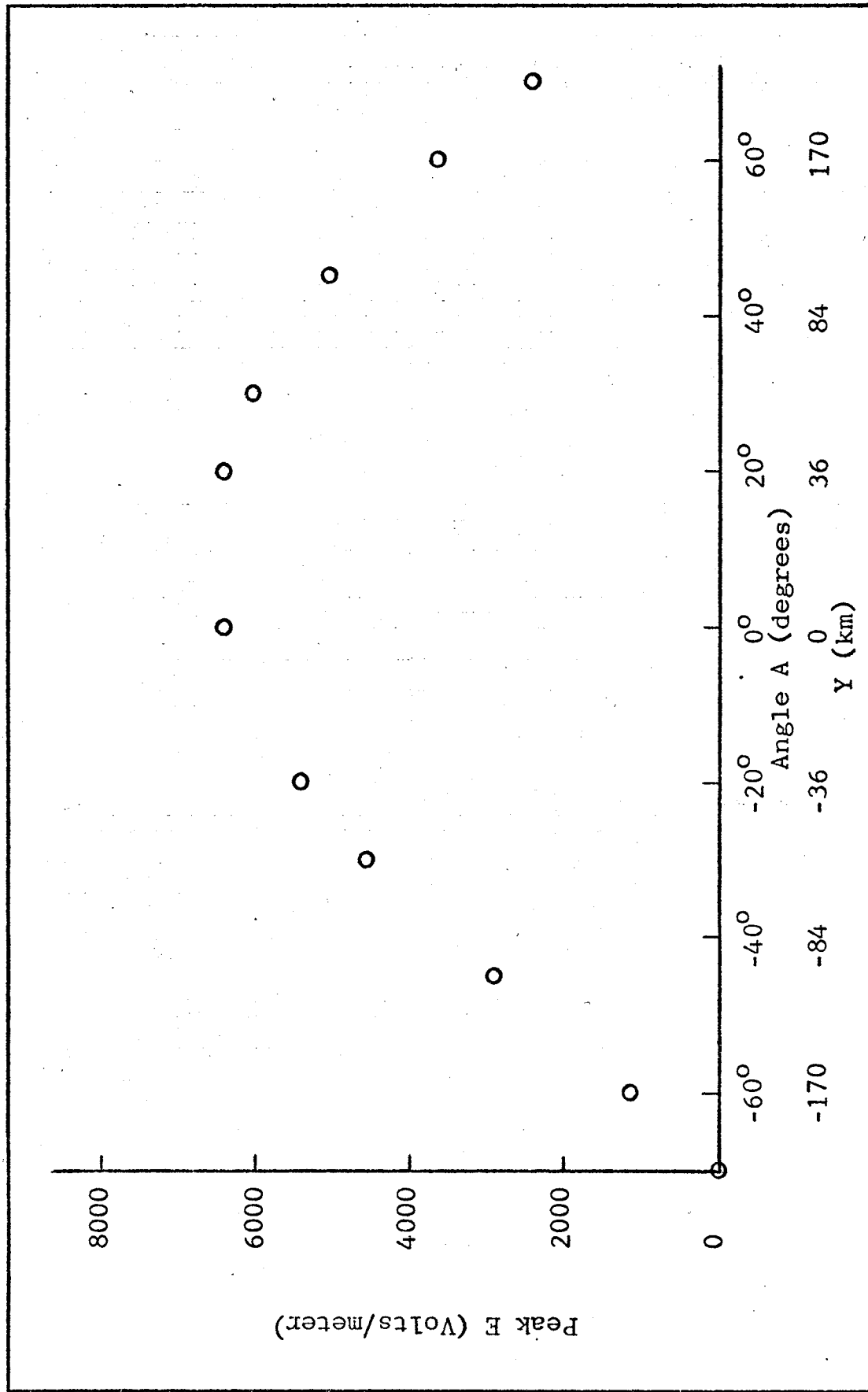


Fig. 7. Variation in Y direction ($X=0$, $Z=0$, $HOB=100\text{km}$, $Y_Y=.001\text{kt}$)

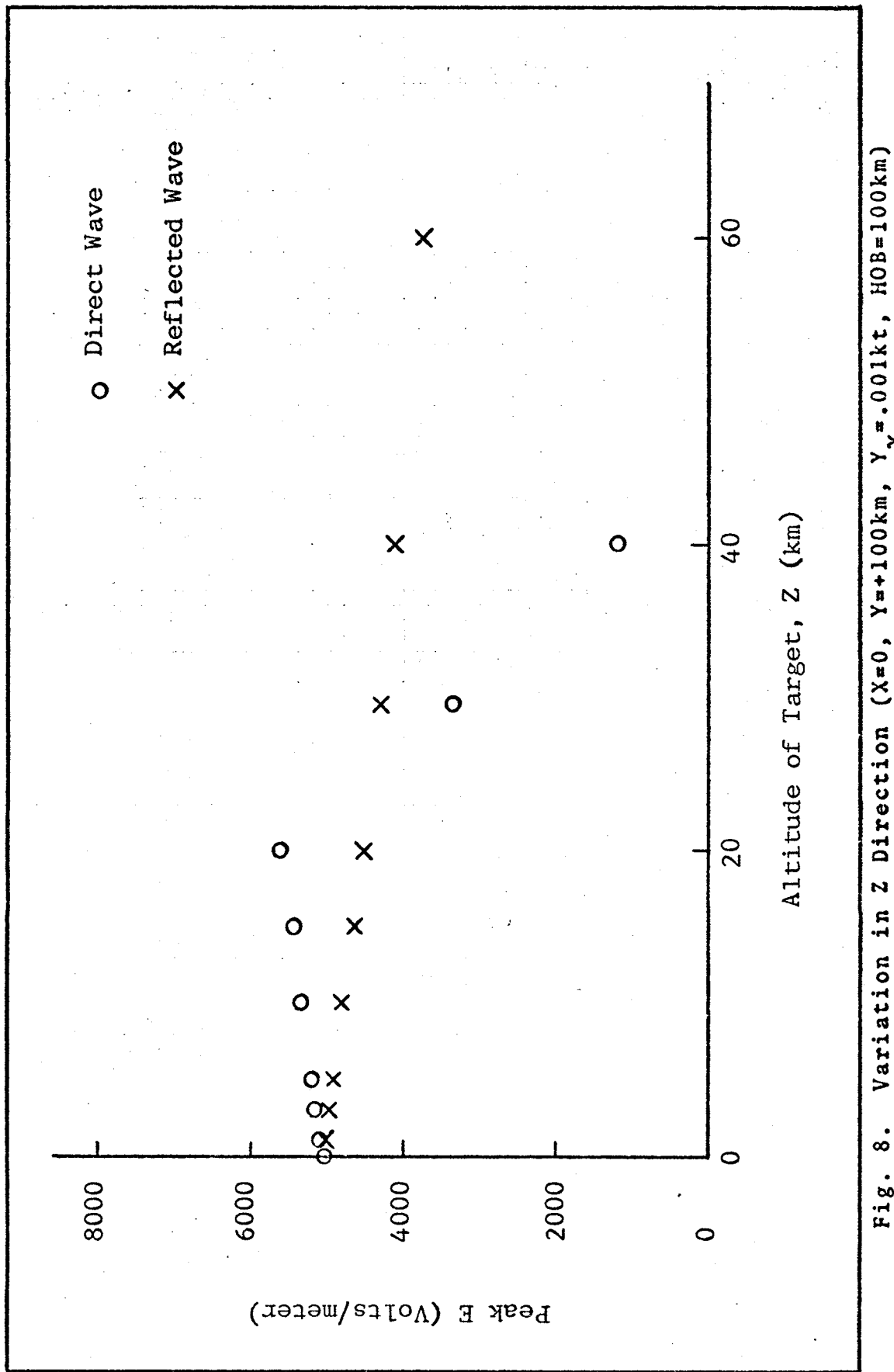


Fig. 8. Variation in z Direction ($X=0$, $Y=+100\text{km}$, $\gamma_\gamma=.001\text{kt}$, $HOB=100\text{km}$)

region. Note that $Y = 100$ km for these runs. As expected, the direct wave falls off rapidly as the target altitude passes through the absorption region, since less of the absorption region contributes to the wave with each increase in altitude. The crossover point where the reflected wave becomes the largest occurred at 25 km in this case. Above ground zero the crossover point was 29.4 km. The altitude of the crossover point is both yield and geometry dependent. It is necessary for the user to calculate both waves whenever there is any doubt which one is the largest.

The reflected wave calculation assumes 100% reflection from the ground and no attenuation in the absorption region or the ionosphere. These assumptions are reasonable if it is recalled that only the high frequency component is being considered and that it requires at least

$$\frac{40 \text{ km}}{3(10)^8 \text{ m/sec}} = 133 \mu \text{ sec} \quad (67)$$

for the wave to leave the absorption region, reach the earth, be reflected, and return to the absorption region. This length of time is enough for a significant number of the free electrons to recombine and reduce the effective conductivity of the absorption region.

The results of variation in HOB are shown in Fig. 9. For all values of HOB attempted below 60 km the code went unstable. Infinite values for E were obtained which resulted in abnormal termination of the calculations. This is

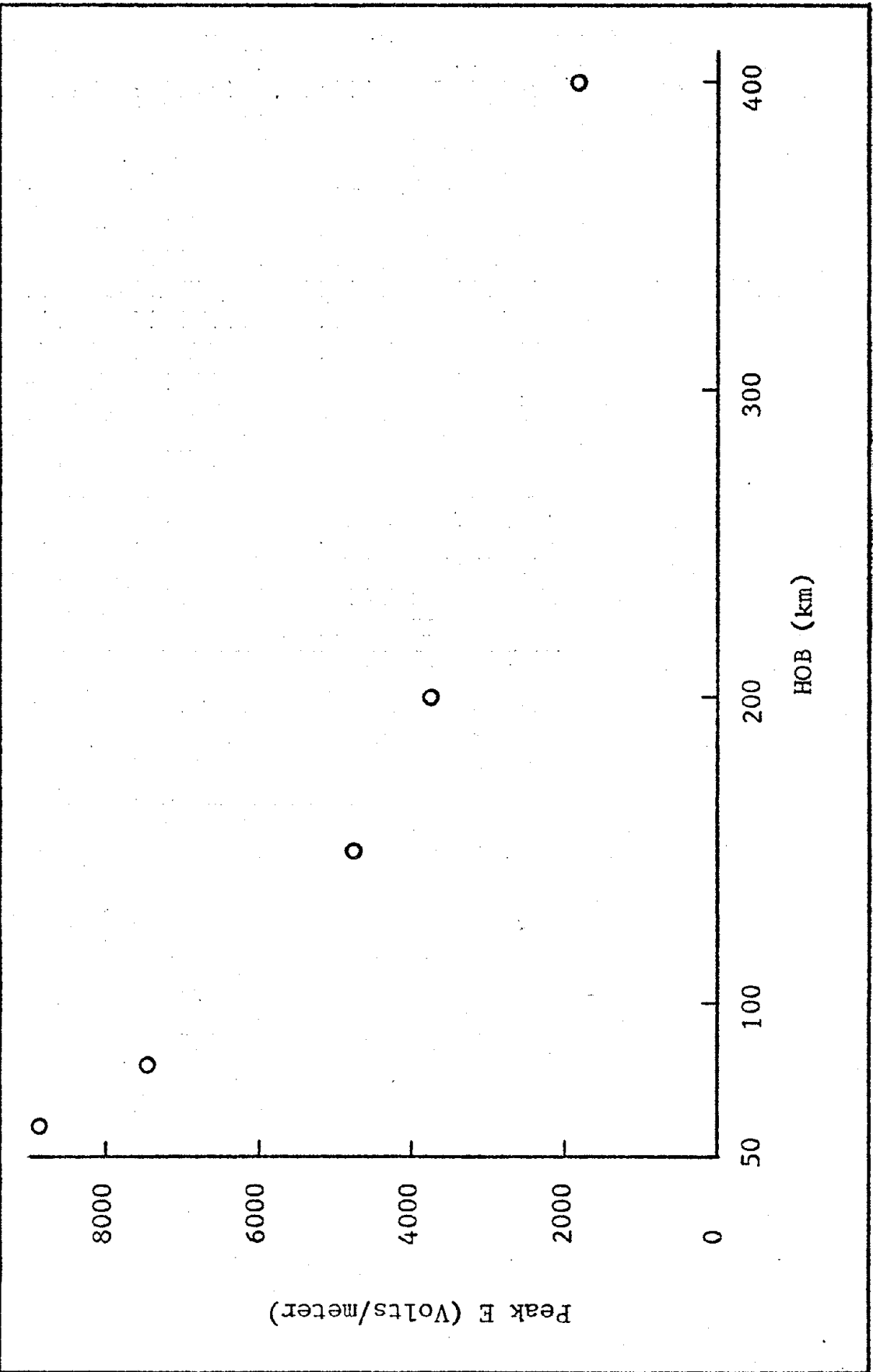


Fig. 9. Variation in Height of Burst ($X=0$, $Y=0$, $Z=0$, $Y_Y = 0.001 \text{kt}$)

expected since the burst is assumed to be distant from the absorption region (equations 9 and 10).

The results of variation in gamma yield are shown in Fig. 10. For all gamma yields attempted above 60 tons the code went unstable, giving infinite values for E. However, the instability always occurred at times later than the natural peak value of E. For example, with 80 tons of gamma yield, the natural peak occurred at 1 shake and the instability occurred at 10 shakes. By using the natural peak value and ignoring the instability, reasonable values for peak E were obtained up to 1 kt of gamma yield.

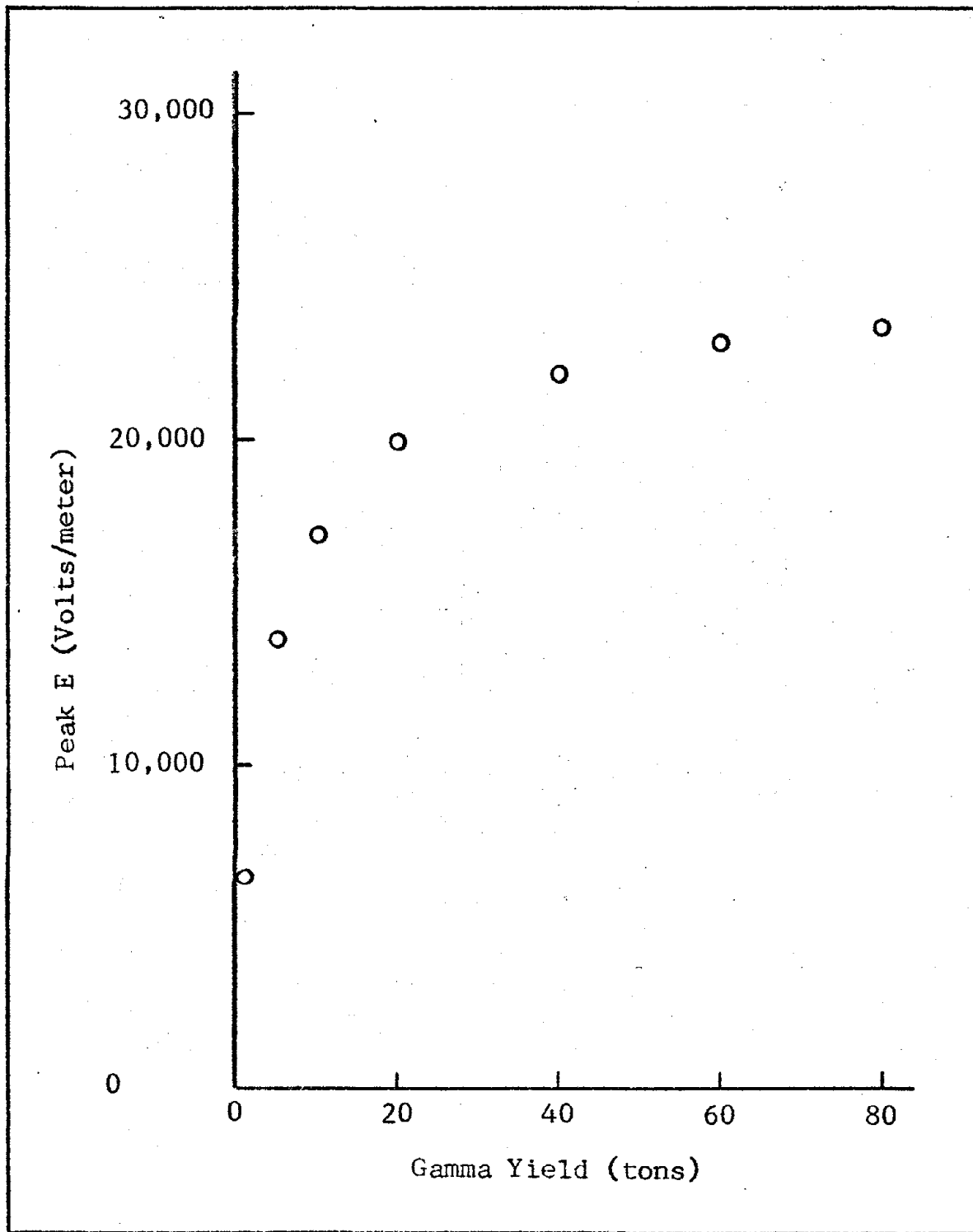


Fig. 10. Variation in Gamma Yield ($X=0$, $Y=0$, $Z=0$, HOB=100km)

V. Discussion and Recommendations

Limitations

Most of the limitations of the code are inherent in the model upon which it is based. Approximations such as a flat earth, a uniform magnetic field, and constant speed Compton electrons can be improved only by changing the model. In addition, the effect of the self generated electromagnetic fields on the motion of the Compton electrons is ignored, as is recombination of both primary and secondary electrons. The possibility of a single gamma ray interacting to produce more than one Compton electron is not allowed. In the absorption region the contribution of the non-propagating radial component of the electric field is neglected. Also, the model is not easily adapted to multi-group gamma transport, or to multiple burst calculations.

The code calculates only the effect of the gamma rays. The user must keep in mind that X-ray generated EMP becomes important for bursts above 100 km.

The code does not account for the increase in altitude of the absorption region for slant angles (angle A in Fig. 1) greater than 60° which is indicated by Latter and LeLevier (Ref 4).

Since 97% of the running time of the code is used for numerical iteration it is not practical to adapt the code to run more than one target at a time. Two targets would

merely double the running time, so it is simpler to just make two runs. Typical requirements are 200 seconds running time with 33000_8 words of central memory on the CDC 6600 computer using NDELR = 50 and TMAX = 20 shakes.

Uses

The code can be used to calculate the peak value of the E field at a target, anywhere on or above ground level, resulting from a nuclear burst above 60 km altitude with a gamma yield up to 60 tons. Either the direct or the ground reflected wave can be calculated. With special care, bursts up to 1 kt of gamma yield can be used.

Recommendations

In the interest of accuracy, the targets should be located such that the slant angle, A, is between -60° and $+60^\circ$.

By accepting a much longer running time the accuracy and hopefully, the stability of the code could be improved by using a smaller step size in the integration of the Compton current equations. Reducing the step size from one tenth of the Compton lifetime to one shake would require approximately ten times as much running time as the code presently requires. This possibility should be investigated further to determine the optimum step size for obtaining the best relationship between accuracy and running time.

Another possibility for increasing the accuracy and stability of the code is to reduce the step size in r. The present code has the capability of dividing the absorption region into 500 steps in r along the line of sight. Of course, the running time required for 500 steps is ten times that required for 50 steps. A modification of the code to allow more than 500 steps would increase the amount of computer core required as well as increasing the running time. This provides another area for investigation to determine the best trade off point between accuracy and running cost.

These two possibilities could be investigated with minor modifications to the present code. However, the computer time required would be considerable.

In addition, there are numerous possibilities for improvements in the model itself. Some of the more important ones are;

Using multigroup gamma transport.

Using multigroup Compton electrons.

Allowing angular distribution of Compton electrons.

Using self consistent electromagnetic fields.

Including the low frequency components.

Each of these would require major modifications to the present code.

Bibliography

1. Kinsley, O.V. Introduction to the Electromagnetic Pulse, Wright-Patterson AFB: Air Force Institute of Technology, March 1971. (GNE/PH/71-4).
2. Karzas, W. J. and R. Latter. "Detection of the Electromagnetic Radiation from Nuclear Explosions in Space", Physical Review, Vol 137, No. 5B, pages 1369-1378, March 8, 1965. (Also published as EMP Theoretical Note 40).
3. Pomranning, G. C. "Early Time Air Fireball Model for a Near-Surface Burst", DNA 3029T, March 1973.
4. Latter, R. and R. E. LeLevier. "Detection of Ionization Effects from Nuclear Explosions in Space", Journal of Geophysical Research, Vol. 68, No. 6, March 15, 1963.
5. Wylie, C. R. Jr. Advanced Engineering Mathematics, New York: McGraw-Hill Book Co. 1966. (Third Edition).
6. Lecture Notes, Electromagnetic Waves, EE 6.30, Air Force Institute of Technology, Wright-Patterson AFB, Summer, 1973. (Course taught by Maj. Carl T. Case.)

Appendix A

EMP Code User's Guide

EMP Code User's Guide

The code is run the same as any other Fortran Extended program, but due to the running time it should be converted to binary form before execution. The plotting subroutine requires an on-line plotter and both linear and log plotting library subroutines.

The input data is read in the following order:

Data card #1, using FORMAT (7F10.0, 215), contains;

X,Y,Z The target coordinates in meters

HOB The height of the burst in kilometers
(60 km \leq HOB)

GAMYLD The gamma yield in kilotons
(GAMYLD \leq 1 kt)

BFIELD The Earth's magnetic field in wb/m²

BANGLE The magnetic field dip angle in degrees

NDELR The number of steps in r taken through
the absorption region (50 \leq NDELR \leq 500)

OUT The output control parameter

Data card #2, using FORMAT (13), contains;

ITER The time period covered by the iterations
in shakes (10 \leq ITER \leq 100) (ITER = TMAX)

Data card #3, using FORMAT (4F10.0), contains;

A Pomranning constant α in inverse shakes

B Pomranning constant β in inverse shakes

RN Pomranning constant N in shakes

TO Pomranning constant τ_0 in shakes

Default values are provided for BANGLE, BFIELD, and NDELR. They are 40° , 0.00002 wb/m^2 , and 50 respectively.

If these default values are desired, zero must be punched in their respective card fields.

The ground reflected wave at the target is obtained by reading in the target altitude, Z, as a negative number. For any target within the absorption region, both the direct and the ground reflected wave should be calculated to determine which one is the strongest.

For values of GAMYLD between 0.06 kilotons and 1.0 kilotons the code will most likely go unstable. This instability occurs after the real peak has been calculated, but the peak value printed out may not be the real peak. Since execution is terminated when the field becomes greater than $1E15 \text{ V/m}$, the array search can result in a false peak value. In this case, the array itself (or the plot) can be used to determine the real peak value.

Increasing NDELR makes the step size in r through the absorption region smaller and the calculation becomes more accurate. However, total running time varies directly with changes in NDELR. For example, using NDELR = 100 instead of NDELR = 50 will approximately double the running time required for NDELR = 50.

There are four output options provided. Option 0 prints out the informative messages, the calculated peak value at the target, the E array, and the τ array. Option 1 adds a linear plot of the first 20 shakes and a log-log

plot of 100 shakes of E as a function of τ at the target. Option 2 includes both Option 0 and Option 1 and adds a printout of E and σ as a function of τ at the bottom of the absorption region. Option 3 deletes the plots from Option 2. The last two options are primarily for debugging since a partial printout is made for each completed iteration even if execution is terminated before the iterations are completed. The first two options are best for production runs.

The only requirements on the Pommranning constants are N must be chosen such that equations (61) and (62) are satisfied, all of them must be positive, and $\alpha > \beta$.

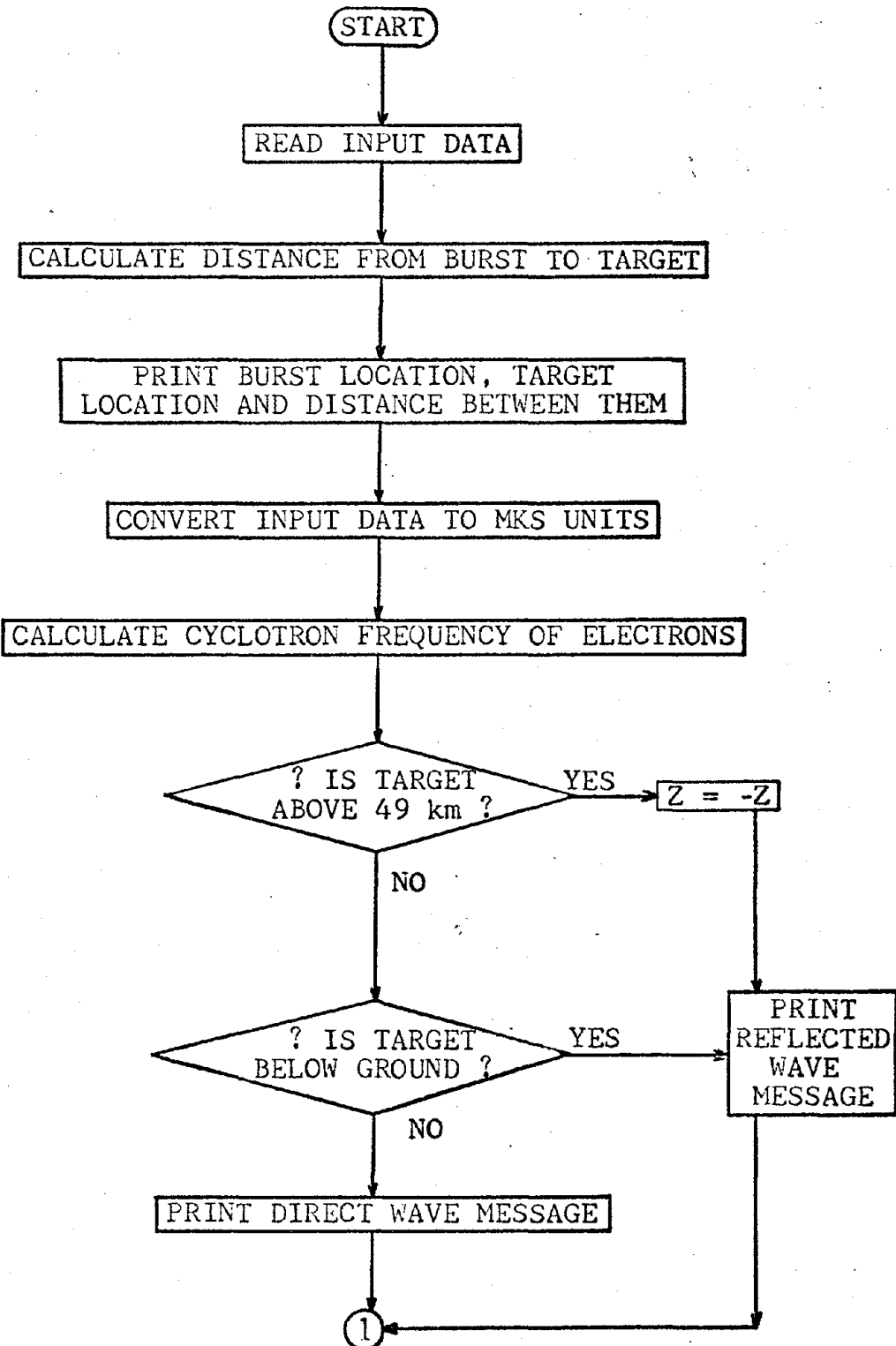
Increasing ITER also increases the running time. For ITER = 10 shakes, running time is approximately 180 seconds on the CDC 6600 computer. For ITER = 100 shakes, running time is approximately 340 seconds. A good compromise, which gives nice looking plots, is ITER = 20 shakes with a running time of approximately 200 seconds.

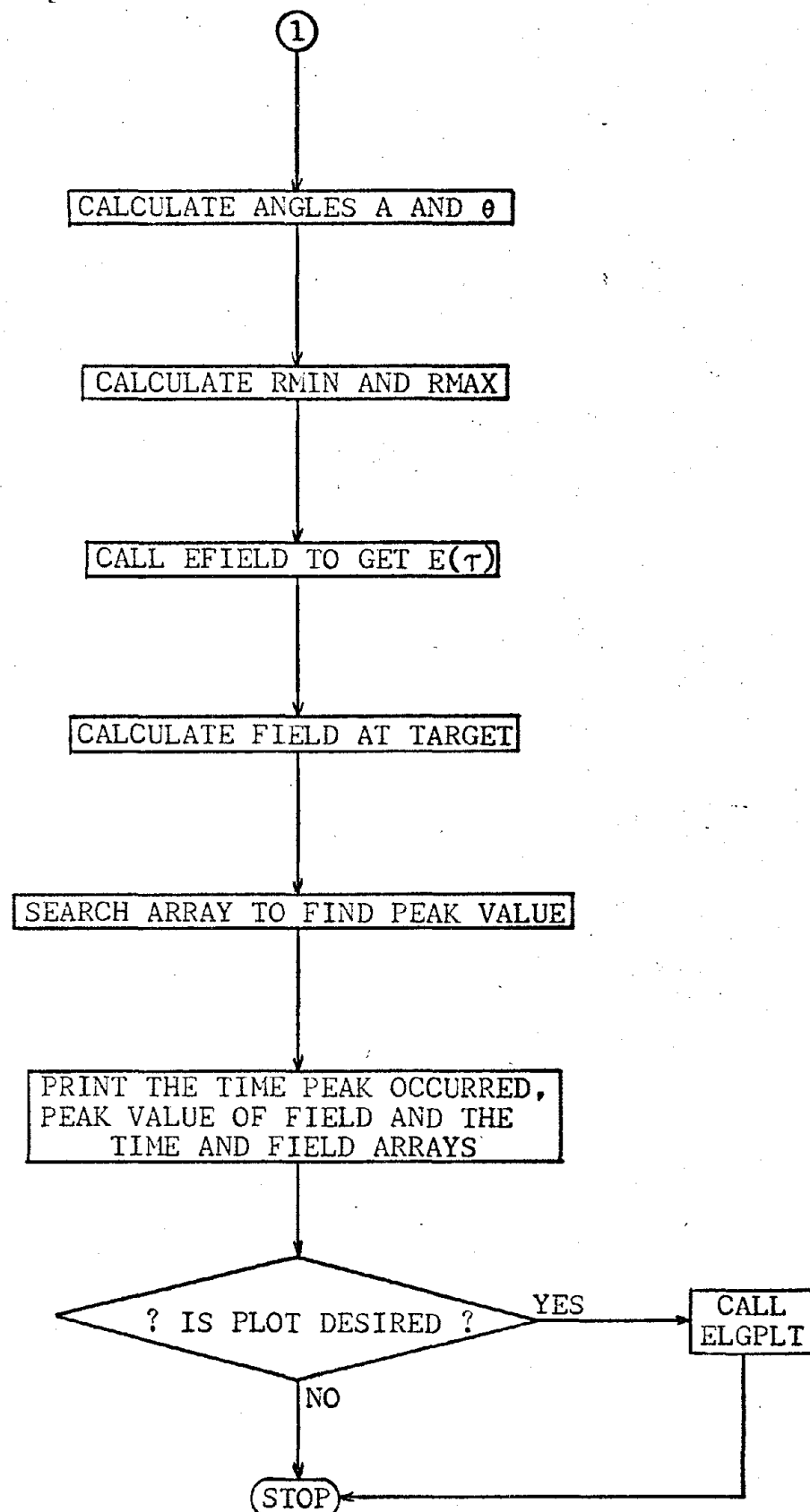
In binary form, the code requires 33000₈ words of core on the CDC 6600 computer.

Appendix B

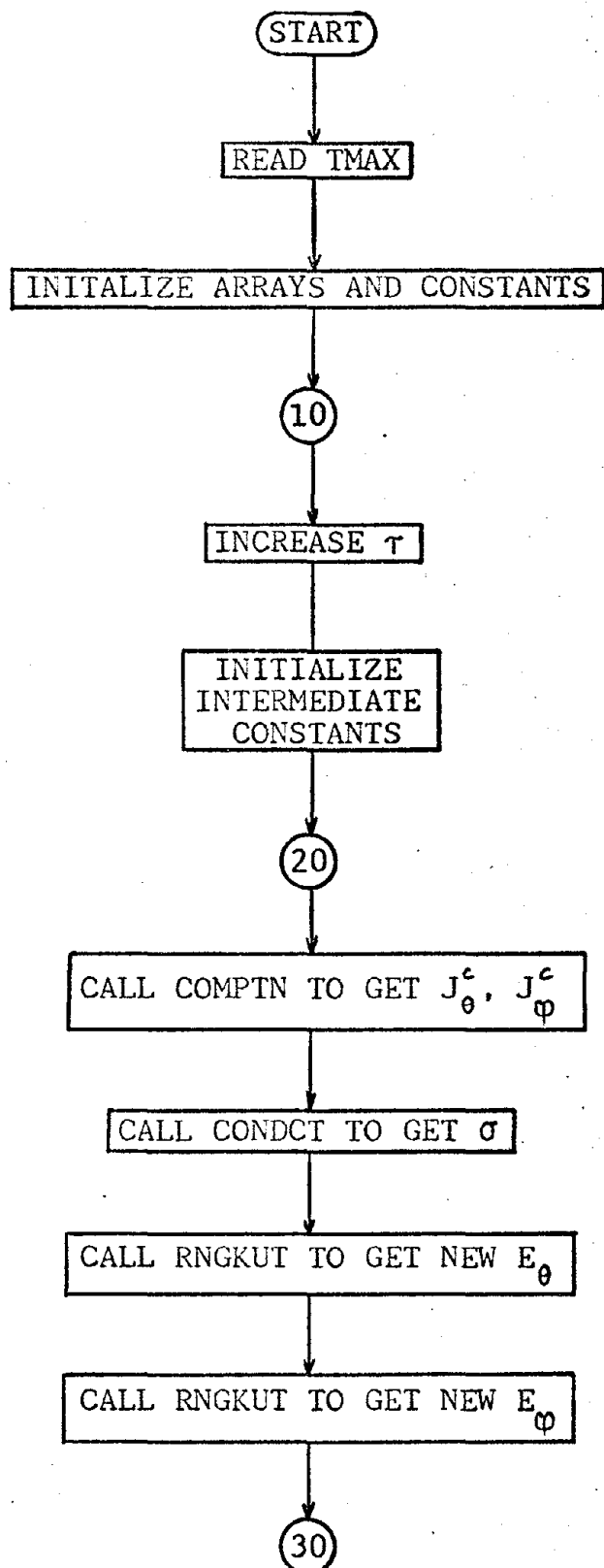
EMP Code Flow Charts

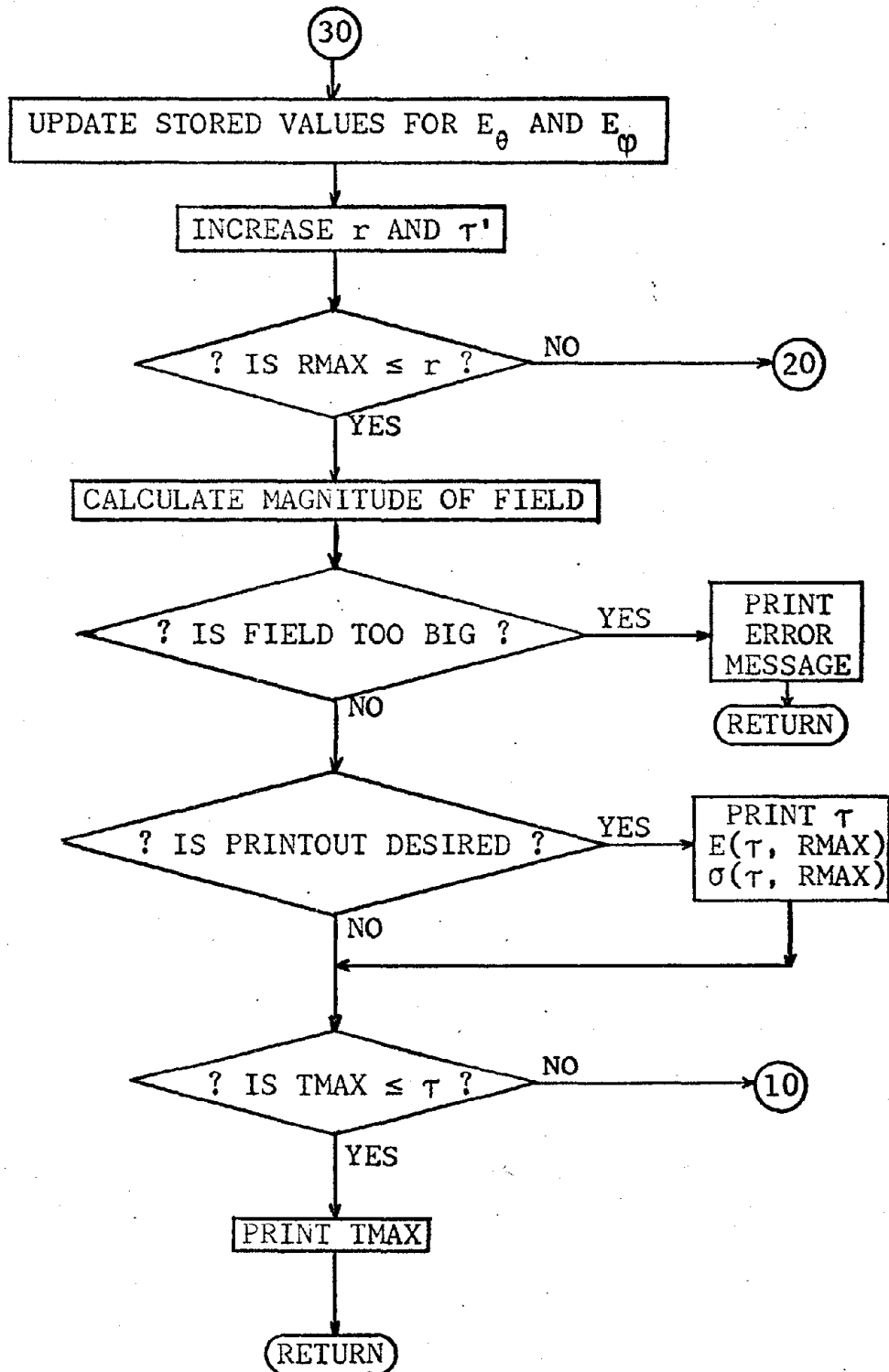
PROGRAM CONTRL



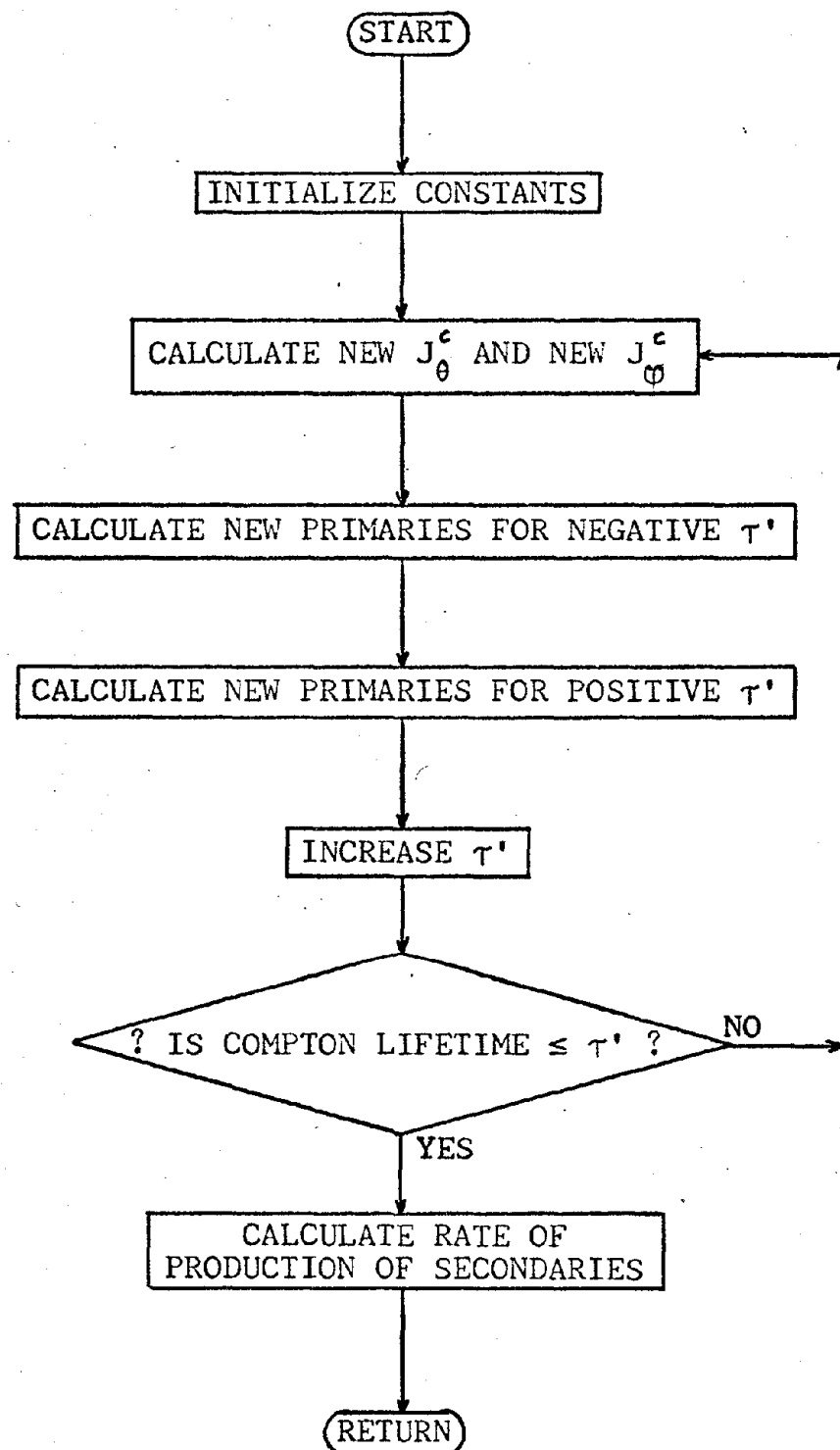


SUBROUTINE EFIELD

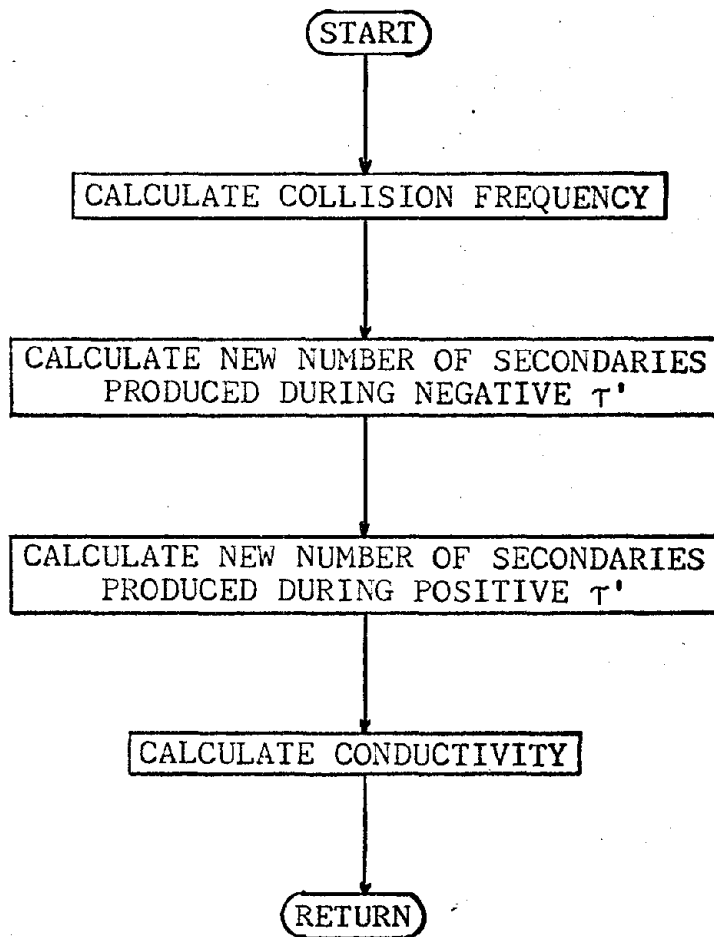




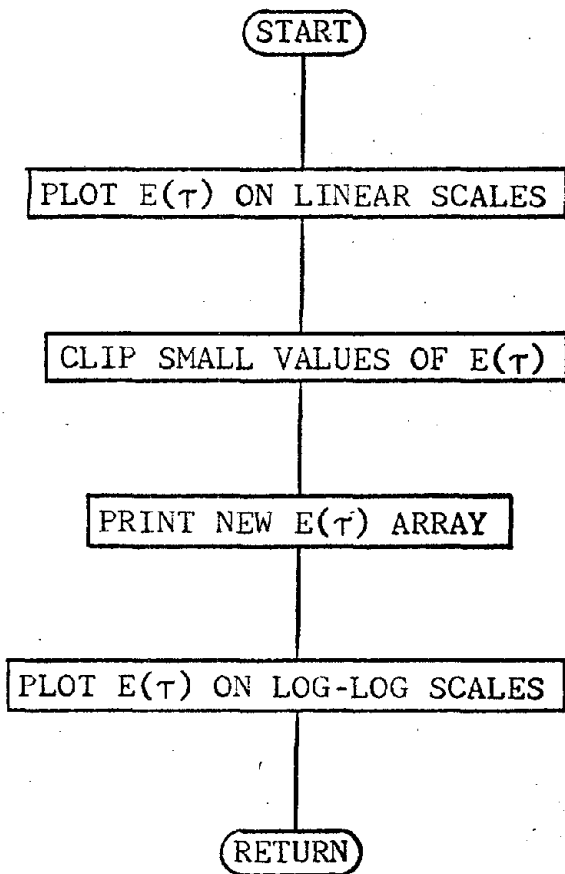
SUBROUTINE COMPTN



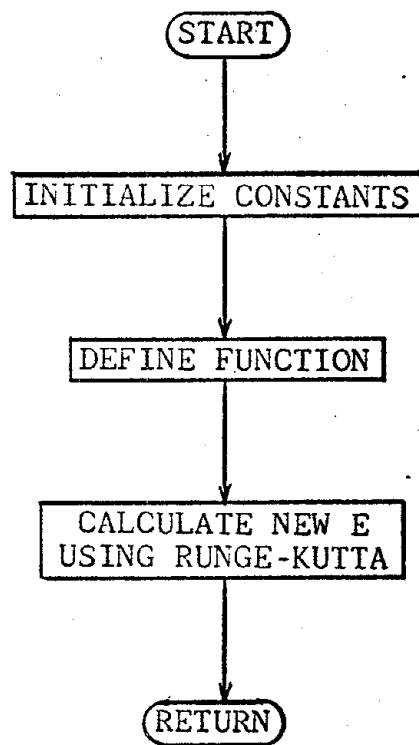
SUBROUTINE CONDCT



SUBROUTINE ELGPLT



SUBROUTINE RNGKUT



Appendix C

EMP Code Listing

```

PROGRAM CNTL (INPUT,CLTFLT,FLOT)
C THIS PROGRAM CONTROLS THE SUBROUTINES
C
COMMON OUT
INTEGER CUT
DIMENSION E(192),TIME(192),STORE2(500)

C X,Y,Z IS THE TARGET LOCATION IN METERS
C FOR THE NORTHERN HEMISPHERE
C X IS MAGNETIC WEST
C Y IS MAGNETIC SOUTH
C Z IS ALTITUDE

C HOE IS HEIGHT OF BURST IN KILOMETERS > 50KM
C GAMYL IS GAMMA YIELD OF BURST IN KILOCNS
C
C BFIELD IS THE MAGNITUDE OF EARTH'S MAGNETIC FIELD IN THE
C ABSORPTION REGION PELCK THE BURST IN WEBERS/SQUARE METER
C
C BANGLE IS THE DIP ANGLE OF THE MAGNETIC FIELD IN DEGREES
C
C NUCLR IS THE NUMBER OF STEPS BETWEEN RMIN AND RMAX
C 50<NUCLR<=500
C
C OUT IS THE OUTPUT CCNTL PARAMETER
C OUT=0 ==> PRINT PEAK VALLE AND ARRAYS
C OUT=1 ==> PRINT PEAK VALLE AND MAKE FLCT
C OUT=2 ==> PRINT EVERYTHING AND MAKE FLCT
C OUT=3 ==> PRINT EVERYTHING
C
C READ 1001,X,Y,Z,HOE,GAMYL,BFIELD,BANGLE,NUCLR,OUT
C R=SQRT (X*X+Y*Y+(HOE*1000.-Z)**2)
C PRINT 2006,GAMYL,HOE,X,Y,Z,R
C
C CNTL 10
C CNTL 20
C CNTL 30
C CNTL 40
C CNTL 50
C CNTL 60
C CNTL 70
C CNTL 80
C CNTL 90
C CNTL 100
C CNTL 110
C CNTL 120
C CNTL 130
C CNTL 140
C CNTL 150
C CNTL 160
C CNTL 170
C CNTL 180
C CNTL 190
C CNTL 200
C CNTL 210
C CNTL 220
C CNTL 230
C CNTL 240
C CNTL 250
C CNTL 260
C CNTL 270
C CNTL 280
C CNTL 290
C CNTL 300
C CNTL 310
C CNTL 320
C CNTL 330
C CNTL 340
C CNTL 350
C CNTL 360

```

```

C      SET UP DEFAULT VALUES
C
C      IF(BANGLE.EQ.0.) BANGLE=40.
C      IF(BFIELD.C.EQ.0.) BFIELD=0.00002
C      IF(NDELR.EQ.0) NDELR=50

C      CONVERT DATA TO MKS UNITS
C
C      HCB=HOB*1000.
C      GAMYLD=2.61625E25*GAMYLC
C      BANGLE=0.017453295*BANGLE
C      CMEGA=1.6E-19*BFIELD/(3.505*1.1E-31)

C      PRINT TYPE OF CALCULATION
C
C      REFLECT=49000.
C      IF(Z.GT.REFLCT)PRINT 2007
C      IF(Z.LT.0.0) PRINT 2008
C      IF(Z.LE.REFLCT.AND.Z.GE.0.) FRINT 2009

C      REFLECTED WAVE CALCULATION ASSUMES 100% REFLECTION
C      AND USES MIRROR IMAGE OF TARGET BELOW GROUND
C      SET Z = -Z IF REFLECTED WAVE IS TO BE USED

C      IF(Z.GT.REFLCT) Z=-Z
C      IF(Z.GT.HOB-1000.) FRINT 2007
C      IF(Z.GT.HOB-1000.) Z=-Z

C      DETERMINE ANGLES
C
C      R=SQRT(X*X+Y*Y+(HOB-Z)**2)
C      A=ACOS((HOB-Z)/R)
C      THETA=ACCS(COS(BANGLE)*Y/R+SIN(BANGLE)*(Z-HCB)/R)

C      DETERMINE RMIN AND RMAX
C
C      CNTL 370
C      CNTL 380
C      CNTL 390
C      CNTL 400
C      CNTL 410
C      CNTL 420
C      CNTL 430
C      CNTL 440
C      CNTL 450
C      CNTL 460
C      CNTL 470
C      CNTL 480
C      CNTL 490
C      CNTL 500
C      CNTL 510
C      CNTL 520
C      CNTL 530
C      CNTL 540
C      CNTL 550
C      CNTL 560
C      CNTL 570
C      CNTL 580
C      CNTL 590
C      CNTL 600
C      CNTL 610
C      CNTL 620
C      CNTL 630
C      CNTL 640
C      CNTL 650
C      CNTL 660
C      CNTL 670
C      CNTL 680
C      CNTL 690
C      CNTL 700
C      CNTL 710
C      CNTL 720

```

```

ZRAIN=5.E4
IF(HOB.LT.ZRMIN) ZRMIN=HCE
TA=(ZRMIN-HOB)/(Z-HOB)
XMIN=TA*X
YMIN=TA*Y
RMIN=SQR(XRMIN**2+YRMIN**2+(ZRMIN-HOB)**2)

ZRMAX=Z
IF(Z.LT.2.E4) ZRMAX=2.E4
TB=(ZRMAX-HOB)/(Z-HOB)
XMAX=TB*X
YMAX=TB*Y
RMAX=SQR(XRMAX**2+YRMAX**2+(ZRMAX-HOB)**2)

C      CALCULATE EFIELD AT ECITCM OF ABSORFTION REGION
C      CALL EFIELD(E,TIME,RMIN,RMAX,NOELR,HOB,A,THETA,OMEGA,GAMYLCE,
1STOP,E2)

C      CALCULATE EFIELD AT TARGET
C      IF(R.LE.RMAX) GO TO 3
DO 1 I=1,190
E(I)=E(I)*RMAX/R
1
C      FIND PEAK VALUE CF EFIELE
C      BIG=0.0
DO 2 I=1,190
IF(E(I).GT.BIG) 4,2
BIG=E(I) $ IT=I
CONTINUE
2
C      PRINT OUTPUT
C      PRINT 2010,TIME(IT)
PRINT 2005,BIG
C      CNTL 730
C      CNTL 740
C      CNTL 750
C      CNTL 760
C      CNTL 770
C      CNTL 780
C      CNTL 790
C      CNTL 800
C      CNTL 810
C      CNTL 820
C      CNTL 830
C      CNTL 840
C      CNTL 850
C      CNTL 860
C      CNTL 870
C      CNTL 880
C      CNTL 890
C      CNTL 900
C      CNTL 910
C      CNTL 920
C      CNTL 930
C      CNTL 940
C      CNTL 950
C      CNTL 960
C      CNTL 970
C      CNTL 980
C      CNTL 990
C      CNTL 1000
C      CNTL 1010
C      CNTL 1020
C      CNTL 1030
C      CNTL 1040
C      CNTL 1050
C      CNTL 1060
C      CNTL 1070
C      CNTL 1080

```

Reproduced from
best available copy.

```

PRINT 2001
PRINT 2002,(TIME(I),I=1,150)
PRINT 2003
PRINT 2004,(E(I),I=1,190)

C      IF DESIRED, MAKE PLCT
C
IF(OUT.LE.0.CR.OUT.GE.3) STCF
CALL ELGFLT(E,TIME,RIG)
STOP

1001 FCFORMAT(7F10.0,2I5)
2010 FCFORMAT(//5X,"PEAK OCCURRED AT",F5.1," SHAKES"//)
2009 FCFORMAT(5X,"DIRECT WAVE IS BEING CALCULATED"//)
2008 FCFORMAT(5X,"REFLECTED WAVE IS BEING CALCULATED"//)
2007 FCFORMAT(5X,"TARGET IS AECUE ASCRIPTION REGION SO REFLECTED WAVE IS"
1 BEING CALCULATED"//)
2006 FCFORMAT("1   THE QURST WITH GAMMA YIELD CF",1PE10.3," KILOCTRS"
1 /5X,"IS AT AN ALTITUDE CF",1PE10.3," KILOMETERS."
2 //5X,"THE TARGET IS AT CCORDINATES",3(5X,1PE10.3)
3 /5X,"WHICH IS",1PE10.3," METERS FRCM THE BURST"//)
2005 FCFORMAT(//5X,"* * * * * PEAK EFIELC AT TARGET IS ",1FE10.3," VOLTS/METER "
1 /5X,"* * * * * PEAK EFIELC AT TARGET IS ",1FE10.3," VOLTS/METER "
2 /5X,"* * * * * PEAK EFIELC AT TARGET IS ",1FE10.3," VOLTS/METER ")
2004 FCFORMAT(19(10(3X,1PE10.3)))
2003 FCFORMAT(//5X,"EFIELD VALUES AT TARGET (IN V/M) ARE"//)
2002 FCFORMAT(19(10(4X,F5.1'4X)))
2001 FCFORMAT("1 TIMES USED (IN SHAKES) ARE"//)
END
CNTL1090
CNTL1100
CNTL1110
CNTL1120
CNTL1130
CNTL1140
CNTL1150
CNTL1160
CNTL1170
CNTL1180
CNTL1190
CNTL1200
CNTL1210
CNTL1220
CNTL1230
CNTL1240
CNTL1250
CNTL1260
CNTL1270
CNTL1280
CNTL1290
CNTL1300
CNTL1310
CNTL1320
CNTL1330
CNTL1340
CNTL1350
CNTL1360

```

```

SUBROUTINE EFIELD(E,TIME,RMIN,RMAX,NDEL2,HOB,A,THETA,JMEGA,GAMYL), EFLD 1J
1STORE2)                                         EFLD 2J
                                                 EFLD 3J
C   CALCULATE THE EFIELD IN THE ABSORPTION REGION          EFLD 4J
                                                 EFLD 5J
                                                 EFLD 6J
                                                 EFLD 7J
                                                 EFLD 8J
                                                 EFLD 9J
                                                 EFLD 10J
                                                 EFLD 11J
                                                 EFLD 12J
                                                 EFLD 13J
                                                 EFLD 14J
                                                 EFLD 15J
                                                 EFLD 16J
                                                 EFLD 17J
                                                 EFLD 18J
                                                 EFLD 19J
                                                 EFLD 20J
                                                 EFLD 21J
                                                 EFLD 22J
                                                 EFLD 23J
                                                 EFLD 24J
                                                 EFLD 25J
                                                 EFLD 26J
                                                 EFLD 27J
                                                 EFLD 28J
                                                 EFLD 29J
                                                 EFLD 30J
                                                 EFLD 31J
                                                 EFLD 32J
                                                 EFLD 33J
                                                 EFLD 34J
                                                 EFLD 35J
                                                 EFLD 36J

C   DIMENSION E(190),TIME(190),STORE2(NDEL2)
REAL JTHETA,JPHI
INTEGER OUT
COMMON OUT,AP,BP,RNP,T02
C   ITER IS TIME OF ITERATION IN SHAES 10<=ITER<=100
READ ITER AND CHANGE IT TO NUMBER OF TIME STEPS          EFLD 100
C   READ 100,ITER
ITER=100+(ITER-10)
C   INITIALIZE ARRAYS AND CONSTANTS
READ 101,AP,BP,RNP,T0P
101  FORMAT(4F10.0)
DO 51 J=1,100
E(J)=0.0 $ TIME(J)=0.1*T0
CONTINUE
DO 71 J=101,190
E(J)=0.0 $ TIME(J)=1.0.+((J-100.)*
CONTINUE
DO 51 L=1,NDEL2 $ STORE2(L)=0.
51  CONTINUE
ETHE=0. $ DELRN=NDEL2 $ T=0. $ DR=1. $ EPHI=0.
CONTINUE
EDELTA=(RMAX-RMIN)/DELRN $ R=2MIN+DE-TA2 $ RNP=1.0E-3*RNP
C   START INTEGRATIONS
OUTSIDE LOOP IS FOR CALCULATION IN RETARDED TIME
INSIDE LOOP IS FOR INTEGRATION IN R AT EACH TIME STEP

```

```

DC 21 I=1,190 $ T=T+(1.E-5)*CT $ TIME(I)=T*(1.E8)
JT=1
IF(I.GT.ITER) GO TO 42
TP=-DELTAR/2*83E8$ CTP=TF 1 SIGMA=0. $ STORE1=0.
DO 31 K=1,NDELR
CALL CCMFTN(JTHETA,JFFI,T,R,P,THETA,OMEGA,FCB,GAMYLD,TP,PRI,FRI2)
CALL CCNOCT(SIGMA,PRI,CTP,CT,HOB,Q,A,STCRE1,STORE2,K,NDELR,FRI2)
CALL RNGKUT(ETHENW,ETHE,R,CELTAR,SIGMA,JTHETA)
CALL RNGKUT(EPHINW,EPHI,R,CELTAP,SIGMA,JFHI)
ETHE=LETENW $ EPHI=EPHINW $ R=R+DELTAR
TP=TP+CTP
CONTINUE
C
C FIND MAGNITUDE CF EFIELE
C
C E(I)=SCRT(ETHE**2+EJFHI**2)
C
C CHECK FOR DIVERGENCE CF SOLUTION
C
C IF(E(I).GT.1.E15) GO TO 52
C IF(I.EQ.100) DT=1.0.
C R=RMIN+DELTAR
C
C IF DESIRED, PRINT OUTFLT
C
C IF (OUT<1.LE.0) GO TO 21
C PRINT 5,I,TIME(I),E(I),SIGMA
C CONTINUE
21
C
C PRINT MESSAGE AFTER TERMINATION OF TIME LOOP
C
C 42 PRINT 201,TIME(ITER)
C RETURN
C
C PRINT MESSAGE AFTER A NORMAL TERMINATION OF TIME LOOP
C

```

```

52 PRINT 301
      FRINT 201,TIME(IT)
      IF(IT.LT.10)RETURN
C      SET LAST 5 VALUES OF EFIELD TO 0.0 TO AVOID INCORRECT FEAK
C      E(IT)=E(IT-1)=E(IT-2)=E(IT-3)=E(IT-4)=E(IT-5)=0.0
      RETURN
100  FCRMAT (I3)
      5   FCRMAT (" I =",I4," TIME =",F6.1," SHAKES E(T,RMAX) =",
      5   11FE10.3," VOLTS/METER SIGMA =",1PE10.3," MHQ/METER")
      201 FCRMAT (//5X,"ITERATION TERMINATED AFTER",F5.1," SHAKES //")
      301 FCRMAT (//15X,"*****/15X,"**** SOLUTION HAS GONE UNSTABLE"
      301 1/15X,"*****//")
      END

```

```

      SUBROUTINE CNDCT(SIGMA,FFI,CTP,DT,HOB,R,A,STORE1,STORE2,K,NCLR,
     1FRI2)
C
C      CALCULATES SIGMA AFTER FINDING
C      NSECCNDARY FROM NPRIMARY
C
C      STCRE1 CCNTAINS INTEGRAL FOR NEGATIVE TAU
C      STCRE2 CCNTAINS INTEGRAL FOR POSITIVE TAU
C
C      DIMENSION STCRE2(NDELR)
C      CCLSN=4.*E12*EXP((R*COS(A)-FCB)/7000.)
C      STORE1=STORE1-PRI*CTP
C      STORE2(K)=STCRE2(K)+PRI2*E1*(1.0E-9)
C      SEC=STCRE2(K)-STORE1
C      SIGMA=(1.6E-19**2)*SEC/(CCLSN*9.11E-31)
C      RETURN $ END

```

```

SUBROUTINE CCMPTN(JTHETA,JPHI,T,R,A,THETA,CMEGA,HOB,GAMYLD,TF,FRI,CMTN 10
1PRI2)
C
C   CALCULATE THE TWO COMPCNTS OF THE
C   COMPTON CURPEN1 AT GIVEN T AND R
C   CALCULATE NUMBER OF PRIMARY ELECTRONS
C
C   JTHETA IS THET A COMPCNT CF COMPTON CURRENT
C   JPHI IS PHI COMPCNT CF COMPTON CURRENT
C   TMAX IS COMPTON LIFE TIME
C   PATH IS ALTITUDE SCALFC COMPTON MEAN FREE PATH
C   TP IS NEGATIVE RETARDED TIME
C   T IS POSITIVE RETARDED TIME
C   PRI IS NUMBER OF PRIMARY ELECTRONS GENERATED DURING TF
C   PRI2 IS NUMBER CF PRIMARY ELECTRONS GENERATED DURING T
C   TPRIME IS VARIABLE CF INTEGRATION
C
C   INITIALIZE CONSTANTS
C
C   REAL JTHETA, JPHI
C   JTHETA=0. $ JPHI=0. $ TFRIME=(5.E-9) $ TMAX=CLIFE(R,A,HOB) $ FRI=0. CMTN 210
C   DT=TMAX/10. $ PATH=309.*EXP((HOB-R*COS(A))/7000.) $ TPRIME=DT$W=DT/2. CMTN 220
C   PRI2=0.
C
C   RUNGE-KUTTA INTEGRATION CF COMPTON CURRENT
C
C   FC 31 K=1,10
C   RK1=DT*CMTHE(T(HOB,R,A,THETA,CMEGA,PATH,I,TFRIME,GAMYLD)
C   RK2=DT*CMTHE(T(HOB,R,A,THETA,CMEGA,PATH,I,TFRIME+W,GAMYLD)
C   RK3=RK2
C   RK4=DT*CMTHE(T(HOB,R,A,THETA+(PK1+2.* (RK2+RK3)+RK4)/6.
C   JTHETA=JTHETA+(PK1+2.* (RK2+RK3)+RK4)/6.
C   RK5=DT*CMPHI (HOB,R,A,THETA,CMEGA,PATH,I,TFRIME,GAMYLD)
C   RK6=DT*CMPhi (HOB,R,A,THETA,CMEGA,PATH,I,TFRIME+W,GAMYLD)
C   RK7=RK6
C   RK8=DT*CMPhi (HOB,R,A,THETA,CMEGA,PATH,I,TFRIME+DT,GAMYLD)
C
C   CMTN 20
C   CMTN 30
C   CMTN 40
C   CMTN 50
C   CMTN 60
C   CMTN 70
C   CMTN 80
C   CMTN 90
C   CMTN 100
C   CMTN 110
C   CMTN 120
C   CMTN 130
C   CMTN 140
C   CMTN 150
C   CMTN 160
C   CMTN 170
C   CMTN 180
C   CMTN 190
C   CMTN 200
C   CMTN 210
C   CMTN 220
C   CMTN 230
C   CMTN 240
C   CMTN 250
C   CMTN 260
C   CMTN 270
C   CMTN 280
C   CMTN 290
C   CMTN 300
C   CMTN 310
C   CMTN 320
C   CMTN 330
C   CMTN 340
C   CMTN 350
C   CMTN 360

```

```

C C
      JPHI=JPHI+(RK5+2.* (RK6+RK7)+RK8)/6.

C C
      RUNGE-KUTTA INTEGRATION OF PRIMARIES

      RKP1=DT*RKCMTN(R,THE TA,OMEGA,TP,TPRIME)
      RKP2=DT*RKCMTN(R,THE THETA,OMEGA,TP,TPRIME+W)
      RKP3=RKP2
      RKP4=DT*RKCMTN(R,THE TA,OMEGA,TP,TPRIME+DT)
      PRI=PRI+(RKF1+2.* (RKF2+RKF3)+RKF4)/6.
      RP1=DT*RKCMTN(R,THE TA,CMEGA,T,TPRIME)
      RP2=DT*RKCMTN(R,THE THETA,OMEGA,T,TPRIME+W)
      RP3=RP2
      RP4=DT*RKCMTN(R,THE THETA,CMEGA,T,TPRIME+DT)
      PRI2=PRI2+(RP1+2.* (RP2+RP3)+RP4)/6.
      TPRIME=TPRIME+DT
      CONTINUE
      31
      C C
      MULTIPLY PRIMARIES BY Q*G(R)/TMAX
      TO OBTAIN RATE OF PRODUCTION OF SECONDARIES
      C C
      PRI=PRI*5.000E4*GOFR(R,A,HOB,PATH,GAMYLD)/TMAX
      PRI2=PRI2*5.0E4*GOFR(R,A,HOB,PATH,GAMYLD)/TMAX
      RETURN $ END

```

```

FUNCTION CMPPHI(HOB,R,A,THETA,OMEGA,PATH,T,TPRIME,GAMYLD)
C
C      CALCULATES F(T,R) FOR RUNGE-KUTTA INTEGRATION
C      OF PHI COMPONENT OF CURRENT
C
C      SOLVE=TOFT(SOLVE)
C      SOLVE=F0FT(SOLVE)
C      SOLVE=SOLVE*(-4.608E-11)*GCFF(R,A,HOB,FATH,GAMYLD)
C      CMPPHI=SOLVE*SIN(THETA)*SIN(OMEGA*TPRIME)
C      RETURN $ END
C
C      CMPPHI=1010
C      CMPPHI=1020
C      CMPPHI=1030
C      CMPPHI=1040
C      CMPPHI=1050
C      CMPPHI=1060
C      CMPPHI=1070
C      CMPPHI=1080
C      CMPPHI=1090
C      CMPPHI=1100

```

```

FUNCTION CMTTHET(HOB,R,A,THETA,OMEGA,PATH,T,TPRIME,GAMYLD)
C
C      CALCULATES F(T,R) FOR RUNGE-KUTTA INTEGRATION
C      OF THETA COMPONENT OF CURRENT
C
C      SOLVE=TOFT(T,TPRIME,THETA,OMEGA)
C      SOLVE=F0FT(SOLVE)
C      SOLVE=SOLVE*(-4.608E-11)*GCFF(R,A,HOB,FATH,GAMYLD)
C      CMTTHET=SOLVE*SIN(THETA)*COS(OMEGA*TPRIME)-1.)
C      RETURN $ END
C
C      CMTTHET=1010
C      CMTTHET=1020
C      CMTTHET=1030
C      CMTTHET=1040
C      CMTTHET=1050
C      CMTTHET=1060
C      CMTTHET=1070
C      CMTTHET=1080
C      CMTTHET=1090
C      CMTTHET=1100

```

```

C SUBROUTINE RNKGUT (E1,E,R,T,SIGMA,COMPTJ)
C
C E(I+1) IS CALCULATED FROM E(I)
C USING THE RUNGE-KUTTA METHOD
C
C DATA (C=3.0E8), (RMU0=12.56637E-7)
C EFUN(R,E)=(1.0/R+C*FMU0*SIN(P/2.0))*E-COMPTJ*C*RMU0/2.
C
C RK1=H*EFUN(R,E)
C RK2=H*EFUN(R+H/2.,E+RK1/2.)
C RK3=H*EFUN(R+H/2.,E+RK2/2.)
C RK4=H*EFUN(R+H,E+RK3)
C E1=E+(RK1+2.*(RK2+RK3)+RK4)/6.
C RETURN $ END
C
C RNK11010
C RNK11020
C RNK11030
C RNK11040
C RNK11050
C RNK11060
C RNK11070
C RNK11080
C RNK11090
C RNK11100
C RNK11110
C RNK11120
C RNK11130

```

```

C FUNCTION RKCMTN(R,THETA,CMEGA,TP,Tprime)
C
C CALCULATES F(T) FOR RUNGE-KUTTA
C INTEGRATION OF PRIMARY ELECTRONS
C
C SCLVE=TOFI(TF,Tprime,THETA,CMEGA)
C RKCMTN=FCFT(SOLVE)
C RETURN $ END
C
C RKCP1010
C RKCP1020
C RKCP1030
C RKCP1040
C RKCP1050
C RKCP1060
C RKCP1070
C RKCP1080

```

```

C GCFR1010
C GOFR1020
C CCFF1030
C GCFR1040
C GOFR1050
C GCFF1060
C GOFR1070
C GCFR1080
C GOFR1090

FUNCTION GOFR (R,A,HOP,FATH,GARYLD)
C
C SOLVES VIRGIN TRANSFER AND USES REACTION RATE TO
C CALCULATE THE NUMBER CENSITY OF RACIAL ELECTRONS
C
C SCLVE=(.0226275/COS(A))*(-1.+EXP(R*COS(A)/7000.))*EXP((-HOB/7000.))
DENOM=12*56637*R*R*PATH*1.E-
GCFR=EXP(-SOLVE)*GARYLD/CENCH
RETURN $ END

```

```

CLIF1010
CLIF1020
CLIF1030
CLIF1040
CLIF1050
CLIF1060
CLIF1070
CLIF1080
CLIF1090

FUNCTION CLIFE (R,A,HOB)
C
C CALCULATES COMFTON LIFETIME AT RADIUS = R
C MAX ACCEPTABLE LIFETIME = 100 SHAKES FOR
C THE KARZAS-LATTER HIGH FREQUENCY APPROX
C
CLIFE=1.0416E7E-8*EXP((1.E-8*R*COS(A))/7000.)
IF(CLIFE.GT.1.E-6) CLIFE=(1.E-6)
RETURN $ END

```

```

FUNCTION TOFT (T,Tprime,Theta,Omega)
C
C   T(T) IS TIME TRANSFORMED TO KARZAS-LATTER FORM
C
C   3=0.358
FIRST=T-(1.-B*(2*Theta)**2)*Tprime
SECOND=B*(SIN(Theta)**2)*SIN(Omega*Tprime)/Omega
TOFT=FIRST+SECOND
RETJRN $ END

```

```

FUNCTION FOFT(T)
C
C   F(T) IS THE POMRANNING MODEL FOR TIME DEPENDENCE
C   OF NUCLEAR WEAPON YIELD IN RETARDED TIME
C
C   INTEGER OUT
COMMON OUT,A,B,RN,D
TSHAKE=1.E8*T
DENOM=(B+A*EXP((A+B)*(TSHAKE-T0)))*RN
FOFT=(A+B)*EXP(A*(TSHAKE-T0))/DENOM
RETJRN $ END

```

```

SUBROUTINE ELGPLOT(EFPLT,TIME,BIG)
C
C      THE FIRST 20 SHAKES OF E(T) IS PLOTTED ON LINEAR SCALES
C
DIMENSION EFPLT(192),TIME(192),E(112),T(112)
MAG = 5 $ SMALL = 0.0
CHECK = 0.0
E0 6 I=1,110
F(I)=EFPLT(T) $ T(I)=TIME(I)
CONTINUE
6   CALL PLOT (0.0,-8.0,-3)
CALL PLOT (2.0,2.0,-3)
CALL SCALE (T ,5.,110,1)
CALL SCALE (E ,5.,110,1)
CALL LINE(T ,E ,110,1,0,0)
CALL AXIS(0.,0.,13H TIME (SHAKES),-13,5.,0.,T (111),T (112))
CALL AXIS(C.,0.,12HEFIELD (V/M),12,5.,90.,E (111),E (112))
CALL AXIS(0.,5.,2H ,2,E.,C.,T (111),T (112))
CALL AXIS(5.,0.,2H ,-2,5.,90.,E (111),E (112))
CALL PLOT(10.0,2.0,-3)
CONTINUE
EPLT 10
EPLT 20
EPLT 30
EPLT 40
EPLT 50
EPLT 60
EPLT 70
EPLT 80
EPLT 90
EPLT 100
EPLT 110
EPLT 120
EPLT 130
EPLT 140
EPLT 150
EPLT 160
EPLT 170
EPLT 180
EPLT 190
EPLT 200
EPLT 210
EPLT 220
EPLT 230
EPLT 240
EPLT 250
EPLT 260
EPLT 270
EPLT 280
EPLT 290
EPLT 300
EPLT 310
EPLT 320
EPLT 330
EPLT 340
EPLT 350
EPLT 360
C
C      SMALL VALUES OF E(T) ARE CLIPPED OFF
C      AND E(T) IS PLOTTED ON LOG-LOG SCALES
C
DO 3 I=1,190
IF((EPLT(I)/BIG).LT.(10.**(-MAG)))2,3
EFLOT(I)=BIG*(10.**(-MAG)) $ CHECK=1.
CONTINUE
3   IF(CHECK.EQ.0.) GO TO 11
PRINT 2005
PRINT 2006,(EFLOT(I),I=1,190)
SMALL=BIG*(10.**(-MAG))
PRINT 2007,SMALL,BIG
CONTINUE
11  CALL PLOT (0.0,-8.0,-3)
CALL FLOT (2.0,2.0,-3)

```

```

CALL LESCAL (TIME, 5.0, 190)          EPLT 370
CALL LESCAL (EPLT, 5.0, 190)          EFLT 380
CALL LGLINE (TIME, EPLT, 190, 0, 0)    EPLT 390
CALL LEAXIS(0., 0., 13HTIME (SFAKES), -13, 5., 0., TIME(191), TIME(192)) EPLT 400
CALL LGAXIS(0., 0., 12HEFIELD (V/M), 12, 5., 90., EPLT(191), EPLCT(192)) EPLT 410
CALL LGAXIS(0., 5., 2H , 2, 5., 0., TIME(191), TIME(192)) EPLT 420
CALL LGAXIS(5., 0., 2H , -2, 5., 90., EPLT(191), EPLT(192)) EPLT 430
CALL PLOTE EPLT 440
RETURN EPLT 450
2005 FCRMAT("1      * * * WARNING! FLOT OF E(T) HAS BEEN CLIPPED * * *") EPLT 460
2006 FCRMAT("/5X,"CLIPPED E(T) IS"//19(10(3X,1PE10.3)/)) EPLT 470
2007 FCRMAT("//" MINIMUM E(T) IS",1PE10.3// MAXIMUM E(T) IS",1FE10.3EPLT 480
1) END EPLT 490
                                         EPLT 500

```

Vita

Terry C. Chapman was born on 21 August 1943 in Vancouver, Washington. He graduated from high school in Manitou Springs, Colorado in 1961. He attended the University of Colorado in Boulder where he was elected to Tau Beta Pi, Engineering Honor Society and Sigma Pi Sigma, Physics Honor Society. He received the degree Bachelor of Science, Engineering Physics and a commission in the U. S. Air Force from the University of Colorado in 1969. After attending communications training, he was assigned to Kelly AFB, Texas as a communications operations officer in 1970. He entered the Air Force Institute of Technology in 1972.

Permanent Address: P.O. Box 1144

Manitou Springs, Colorado 80829

This thesis was typed by Ladonna Stitzel.

Numerical Simulation of the HEMP Environment

Cui Meng, *Member, IEEE*

Abstract—This paper develops the program MCHII, numerically simulating the physical process of Compton electron currents scattered by the interaction of γ rays with ambient air molecules radiating the early time electromagnetic pulse (E1) during the high altitude nuclear explosion. The paper discusses the waveform characteristics of the electromagnetic pulse E1 as it propagates toward the ground from beneath the explosion point during the high altitude nuclear explosion, and provides a detailed study with regard to the influence of explosion height, energy, and γ spectrum. Numerical simulations are used to present the waveform characteristics of the electromagnetic pulse after going through the ionized layer above the explosion point after the high altitude nuclear explosion, and the paper presents the distribution of high altitude electromagnetic pulse waveform amplitudes at satellite orbits.

Index Terms—Compton scattering, geomagnetic field, HEMP, ionosphere.

I. INTRODUCTION

IN publications of IEC SC 77C standards, high-power EM includes the high altitude electromagnetic pulse (HEMP), high-power microwaves, and lightning EMP, etc. [1]. Of these environments, HEMP covers all areas within the visual field of the explosion point and affects the widest scope. With high field intensity and abundant frequency spectra, HEMP couples to electronic systems from front-door and back-door, leading to failure and breakdown of electronic equipment, communication interrupt, and dysfunction of command. It constitutes the difficult and key points in electromagnetic protection and reinforcement. Therefore, it is important to understand the physical properties of the HEMP and to provide standard waveforms of the HEMP environment.

The physical processes involved in a nuclear explosion include nuclear radiation and may also incite strong EMP signals. Such a physical mechanism had been predicted by the physicist Fermi prior to the first nuclear test in U.S. In subsequent high-altitude nuclear explosion tests, HEMP signals were observed. In addition several publications of the past have indicated that it is possible to calculate HEMP at the earth's surface using computer modeling [15], [16]. Consequently, HEMP signals are likely to play an important role of positioning, timing, and compliance identification for nuclear radiation monitoring [2]. When the explosion center is in or below the ionosphere, the lower frequency components of the HEMP signals are obstructed due to the existence of an ionized layer in the air over the earth; the

high-frequency portion is chromatically dispersed in the ionized layer. It is therefore necessary to study the feasibility of HEMP monitoring at satellite orbits [3], [4].

II. PHYSICAL MECHANISM OF HEMP GENERATION

In the IEC 61000-2-9 standard [14], HEMP falls into three types, i.e., early-time, mid-time, and late-time HEMPs, or E1, E2, and E3, respectively. When a nuclear device explodes, the instantaneously emitted γ rays and X rays crash into the ambient gas atoms, knocking out the electrons in the atoms, which fly outward in the radial direction to give rise to “Compton currents.” Influenced by atmosphere density, the weapon system, geomagnetism, and the water vapor in the air, the nuclear explosion is not spherically symmetric. Therefore, “Compton currents” will oscillate and radiate a high power electromagnetic pulse, which is called E1. HEMP incited by the interaction of γ rays generated by neutrons in the device radiation with the air is called E2. In addition, the “fireball” generated from the nuclear explosion is a high temperature, high-pressure plasma. The “fireball” excludes the magnetic lines of force of the earth. When the “fireball” expands at a high speed, the magnetic lines of force are compressed; when the “fireball” disappears, the magnetic lines of force return to normal. Such compression and restoration of the magnetic lines of force will arouse electromagnetic radiation inside the earth, which is called E3.

When the point of a nuclear explosion is at high altitude, the instantaneously radiated X rays, γ rays, and neutrons propagate energy under the explosion point. In this area, γ rays act with air molecules to incite Compton electrons. These electrons deflect with the action of geomagnetic field, and the resultant transverse currents draw out transverse electric field when they are transmitted to the Earth's surface. This is the generation mechanism of early-time HEMP known as E1 (see Fig. 1).

III. PHYSICAL MODEL OF CALCULATION

A. Selection of Coordinates

This calculation only included the process of the interaction of Compton electrons incited by γ rays with the geomagnetic field to create the electromagnetic radiation E1. The early-time HEMP incited in this process has the strongest amplitude and abundant frequency spectra.

Fig. 2 shows the geographic structure during the nuclear explosion. In the high altitude nuclear explosion, the γ pulse released from nuclear devices will interact with ambient thin air when it radiates outward, and will scatter Compton-electron currents. Thanks to their huge energy, Compton electrons move forward at a speed close to c , the velocity of light. Due to the very thin air at high altitude, these electrons have a long range. Their movement trail will be violently deflected by the geomagnetic

Manuscript received August 30, 2012; revised March 19, 2013; accepted March 27, 2013. Date of publication May 29, 2013; date of current version June 11, 2013.

The author is with the Key Laboratory of Particle and Radiation Imaging, Ministry of Education, Department of Engineering Physics, Tsinghua University, Beijing 100084, China (e-mail: mengcui@mail.tsinghua.edu.cn).

Color versions of one or more of the figures in this paper are available online at <http://ieeexplore.ieee.org>.

Digital Object Identifier 10.1109/TEMC.2013.2258024

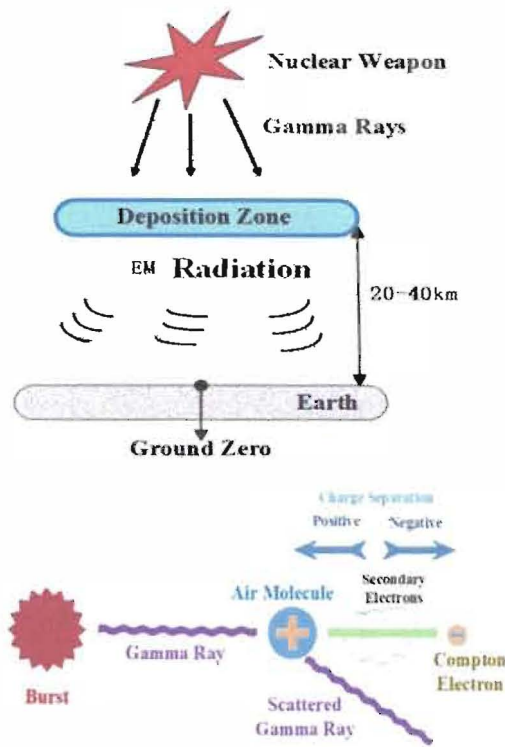


Fig. 1. Generation mechanism of HEMP for the early-time EI.

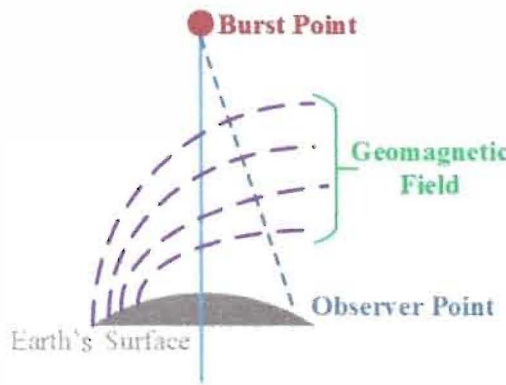


Fig. 2. Geographic location of high altitude nuclear explosion.

field. Thus, Compton currents will have both a radial component J_r and transverse components J_θ and J_ψ in the direction of θ and ψ . If the explosion is axisymmetric to its environment, the radial component J_r and the component J_θ in the direction of θ will incite transverse magnetic waves; the current J_ψ in the direction of ψ will incite transverse electric waves.

The coordinates r, θ, φ are used, with the origin located at the explosion center, and the direction of the polar axis (i.e., axis z for $\theta = 0^\circ$) coinciding with that of geomagnetic field B_0 , i.e., pointing down to the ground (in the Northern Hemisphere). The inclined angle between the geomagnetic field and the vertical axis of ground is supposed to be θ_0 . In other words, the magnetic inclination is $\pi/2 - \theta_0$. In this paper, values $\theta_0 = 30^\circ$ and $\varphi_0 = 0^\circ$ are used in the numerical calculation.

B. Mathematic Equation

The measurement unit of Gauss, cm, g, s, i.e., the static unit for electric charge and electric field was used. The electromagnetic unit was used for electric current and magnetic flux density. Now, the electromagnetic field at any point in the space shall satisfy the Maxwell simultaneous differential equations

$$\frac{1}{c} \frac{\partial \vec{B}}{\partial t} = -\nabla \times \vec{E} \quad (1)$$

$$\epsilon\mu \frac{\partial \vec{E}}{\partial t} + \mu(4\pi\sigma \vec{E} + 4\pi \vec{J}) = \nabla \times \vec{B} \quad (2)$$

$$\nabla \cdot (\sigma \vec{E} + \vec{J}) + \frac{\partial \rho_f}{\partial t} = 0 \quad (3)$$

$$\nabla \cdot \vec{B} = 0. \quad (4)$$

Considering the electric current J and the secondary electron n_{sec} after the counteraction of the geomagnetic field, the expression is as follows [5]:

$$J_r(r, \theta, \varphi, \tau) \approx -\frac{e_q}{c} \epsilon g(r) \int_0^{R_e/\beta} d\tau' \dot{f}_\gamma(\tau - \chi(\tau')) \times (\cos^2 \theta + \sin^2 \theta \cdot \cos \omega \tau') \quad (5)$$

$$J_\theta(r, \theta, \varphi, \tau) \approx -\frac{e_q}{c} \epsilon g(r) \int_0^{R_e/\beta} d\tau' \dot{f}_\gamma(\tau - \chi(\tau')) \times \sin \theta \cdot \cos \theta (\cos \omega \tau' - 1) \quad (6)$$

$$J_\varphi(r, \theta, \varphi, \tau) \approx -\frac{e_q}{c} \epsilon g(r) \int_0^{R_e/\beta} d\tau' \dot{f}_\gamma(\tau - \chi(\tau')) \times \sin \theta \cdot \sin \omega \tau' \quad (7)$$

$$n_{sec}(r, \theta, \varphi, \tau) \approx \frac{q}{c} \frac{g(r)}{R_e} \int_{-\infty}^{\tau} d\tau' e^{-\alpha(r-\tau')} \times \int_0^{R_e/\beta} d\tau'' \dot{f}_\gamma(\tau' - \chi(\tau'')) \quad (8)$$

where

$$g(r) = \beta \frac{\exp(-\int_0^r \frac{dr}{\lambda(r, \theta, \varphi)})}{4\pi r^2 \lambda(r, \theta, \varphi)},$$

$$\lambda(r, \theta, \varphi) = \frac{\lambda_0 \rho_0}{\rho(r, \theta, \varphi)},$$

λ_0 is the γ mean free path at the explosion center (cm); ρ_0 is the air density at the center of explosion (mg/cm^3); $\rho(r, \theta, \varphi)$ is the air density of a source point with coordinates (r, θ, φ) (mg/cm^3); $R_e = R_{e0} \cdot \rho_0 / \rho(r, \theta, \varphi)$; R_{e0} is the j mean range of a Compton electron or photoelectron at the explosion center (cm); $\beta = v_0/c$, v_0 is the initial speed of a Compton electron or photoelectron (cm/s); $\omega = (e_q \cdot B_0 / m_e c^2) \sqrt{1 - \beta^2}$ represents the Larmor frequency (cm^{-1}); $e_q = 4.8 \times 10^{-10}$ represents the absolute value of the electric charge of an electron; m_e is the rest mass of the electron; $\alpha = \alpha_0 (\rho(r, \theta, \varphi) / \rho_0)^2$; α_0 is the rate of attachment of an electron to an oxygen molecule at the explosion center; $q = (\bar{E}_e / 33) \times 10^6$; \bar{E}_e is the average energy

of Compton electrons (MeV); and $\dot{f}_\gamma(\tau)$ is the rate of change of γ s from the device over time (γ photon/s).

The motion equation of secondary electrons in the electric field is taken into account to find out the expression of conductivity as follows, where v_c represents the collision frequency [6]:

$$\sigma(\tau) = \frac{n_{sec}(\tau)}{mv_c} e^2. \quad (9)$$

As the range of a γ ray is close to zero at 20 km above the ground, no new electric field will be generated any longer. The outer boundary for the calculation is selected at 20 km above the ground. Then the electric field reaches the ground in the form of plane wave. The electric field near the ground is calculated with the following formula:

$$E = \frac{E_{r\max} \cdot r_{\max}}{r_{\text{grd}}} \quad (10)$$

where r_{\max} means the distance of explosion point to the location of 20 km above the ground and r_{grd} means the distance from the explosion point to the ground.

IV. RESULTS OF CALCULATIONS

A. Waveform Characteristics and Amplitude Distribution Laws of HEMP on the Ground

Through calculations we found that, early-time HEMP has the property of a steep rise time and a slightly slower trailing time; the maximum electric field on ground is located in the area of 1–2 explosion heights to the south of the burst point on the ground; the area of minimum electric field is located at 50 km to the north of the burst point on the ground, about one magnitude smaller than the maximum value, as shown in Table I. This depends upon the inclined angle between the motion trail of the Compton electrons in the transmission direction and the geomagnetic field. If the inclined angle is smaller, the excited Compton currents will be smaller, and the field intensity will be smaller; if the inclined angle is bigger, the field intensity will be bigger. For a high altitude explosion at 100 km, the location of 50 km to the north of the projection point of explosion center on the ground is precisely the point of intersection of the geomagnetic line at the explosion center with the ground. The area of 1–2 explosion heights to the south is just the area with an inclined angle of 90° with the geomagnetic line at the explosion center.

Peak electric fields in the west–east directions from the explosion center are symmetrically distributed, with identical waveforms in all fields. This can be explained with a mathematic model. In the west–east direction, φ values are different at symmetrical points, but θ values are identical. In the calculation, φ only appears in the calculation of height. Heights at symmetrical points are identical. Consequently, the results of calculation should be identical. Fields in the direction of E_r cannot radiate outward, so they have a value of zero.

The half width of the time waveform is related to the distance from such point to the projection point of the explosion center on the ground. The smaller this distance (the smaller θ), the narrower the half width of the waveform; HEMP has high

TABLE I
THE ELECTRIC FIELD PEAK VALUE DISTRIBUTED ON THE GROUND FROM A 100 km HOB, 1 MT YIELD BURST

Location on the Ground (Projection Point on the Ground from the Explosion Center)	Peak Electric Field E_ψ (V/m)
50 km to the north	2866
26 km to the north	11447
Ground zero	20777
57.7 km to the south	35494
100 km to the south	40042
173 km to the south	40227
247 km to the south	37071
290 km to the south	34802
514 km to the south	30796

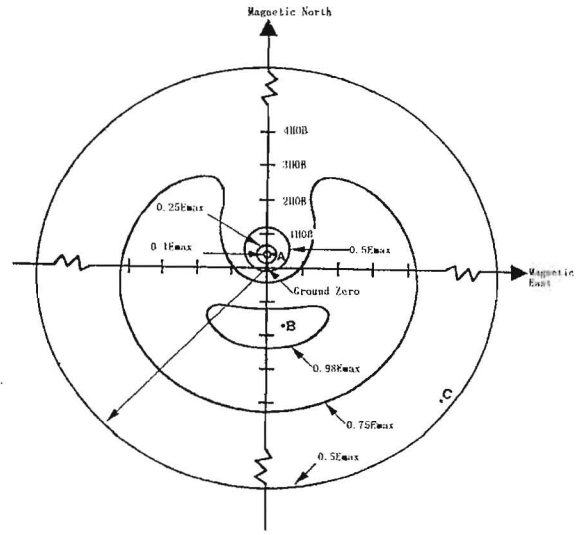


Fig. 3. Typical variations of peak electric fields on the Earth's surface for a high altitude nuclear burst.

electric field amplitudes both in the deposition region and on the ground, ranging from 1 to 100 kV/m (see Table I).

This is consistent with IEC Standard 61000-2-9 published in 1996 [14], as shown in Fig. 3.

On the transmission path from the burst point to the ground, the closer it is to the ground, the narrower the half width of the time waveform. See Fig. 4. The pulsewidth decreases from hundreds of nanoseconds to dozens of nanoseconds. The half width of waveform is generally 20–30 ns near the ground. This is because the closer it comes to the earth's surface, the greater the air density, the greater the value of air conductivity, the faster the low-frequency components at the tail of the waveform decay, and the half width therefore gets smaller.

B. Influence of the Height of Explosion

This paper includes the calculation of explosion heights from 100 to 500 km. The field intensity declines slightly as the explosion height rises as shown in Fig. 5. This is consistent with

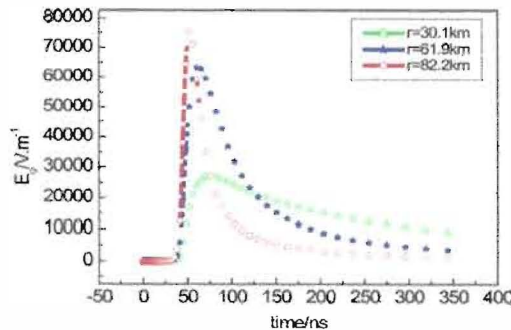


Fig. 4. Waveform of the electric field at different distances from the burst point, $\Psi = 180^\circ$, $\theta = 90^\circ$.

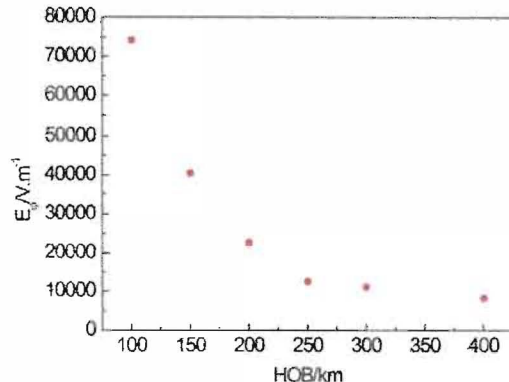


Fig. 5. Relationship between the field strength and HOB (distance from ground zero is 54 km).

the calculation result in the literature [9]. The energy of γ rays from the explosion decays along the radial direction at the rate of $1/4\pi r^2$. The greater the height of explosion, the greater the distance to the energy deposition area, the greater the attenuation, and the lower the energy of γ rays deposited, thus the weaker the induced EMP.

C. Influence of the Explosion Energy

The electric field peak rises as the explosion energy increases. But their relationship is nonlinear as shown in Fig. 6. The peak field intensity of a 2 MT TNT yield is 59 772 V/m and that of a 3 MT TNT equivalent energy is 76 171 V/m.

The figure shows that the slope of the curve decreases as the energy increases; the slope of curve when the energy is small is greater than that when the energy is great.

D. Influence of Rising Time of the γ Rays

In the foregoing calculations, every rising leading edge of γ ray is 7 ns, and the half width of the γ ray waveform is about 200 ns. But the calculations in the IEC standard (see Fig. 8) were conducted when the leading edge of γ ray is 2 ns, and the half width is about 15 ns. It is also noted that the total gamma ray yields for all calculations shown in this paper assume that each gamma ray yield is 0.1% of the total explosion yield. We selected the 2 ns leading edge γ time spectrum for another calculation and found that the rise time of HEMP is closely correlated to the

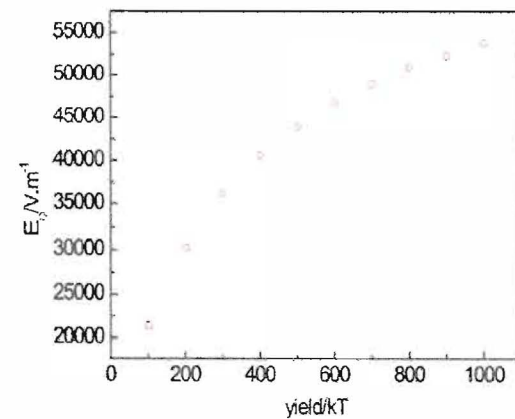


Fig. 6. Distribution of the electric field peak at 110 km from the explosion center with explosion height of 100 km, for different energies, $\theta = 90^\circ$ straight South of the explosion point.

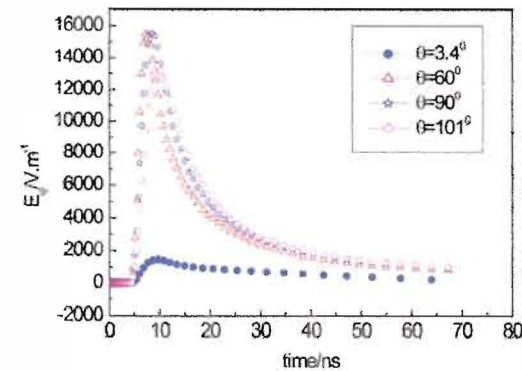


Fig. 7. Calculation result for a 2 ns leading edge of γ rays.

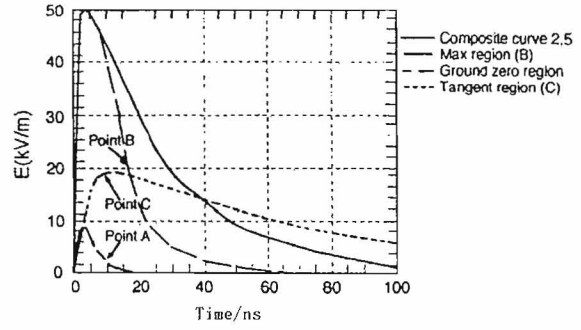


Fig. 8. Recommended waveform in IEC 61000-2-9 [14].

rise time of γ rays, as shown in Fig. 9. The rise time of HEMP will not be faster than that of γ rays, but they are similar. The rise time presented in Fig. 7 is approximately 2.5 ns, with a half width of 10 ns.

E. Transmission Laws of HEMP Above the Explosion Center

To obtain HEMP parameters on satellite orbit, it is necessary to study the generation laws of HEMP in the upward transmission direction from the burst point. The calculation process was a bit different from that of downward transmission. It is necessary to introduce an earth-fixed coordinate system as

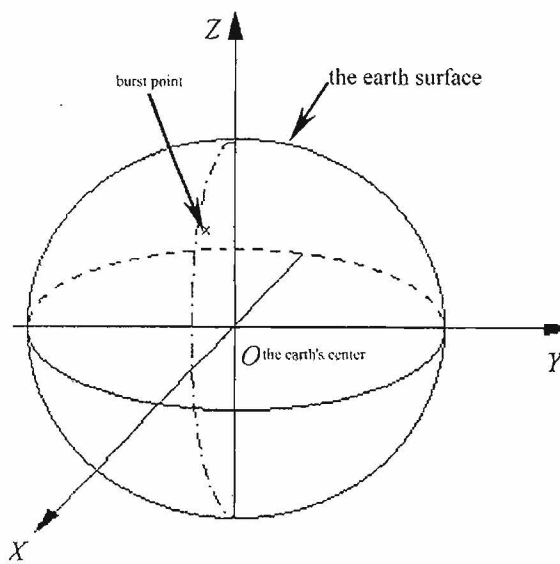


Fig. 9. Earth-fixed coordinate system.

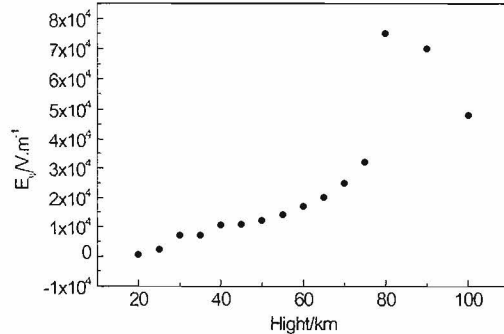


Fig. 10. Changes of the electric field intensity at different HOBs over the explosion center, with a 1 MT yield.

opposed to the foregoing spherical coordinates. As the polar axis of spherical coordinates goes along the direction \vec{B}_0 , and does not coincide with the vertical line of earth surface, there is no simple corresponding relation between the height (h) from the point of origin (r, θ, ψ) to the ground and the value of r . When waves are transmitted to the satellite orbit and when the satellite height is comparable to the earth's radius, the earth surface will not look like a flat surface. Then the position of any point on the satellite orbit in the spherical coordinate system cannot be expressed with a simple formula. The earth-fixed coordinate system is introduced (see Fig. 9) with its origin O at the earth's center, the flat surface XOY coinciding with the earth orbit surface. Axis OX coincides with the Greenwich meridian line. Axis OZ coincides with the polar axis of the earth. Thus, it will not be hard to find the position of points from the explosion center to a synchronous satellite orbit in the spherical coordinate system [13].

The calculation process was adjusted to provide the following result. Fig. 10 presents the curve of relation between the peak value of electric field and the height of explosion.

In addition, the calculation found that the electric field peak rises as the power increases. But their relationship is nonlinear

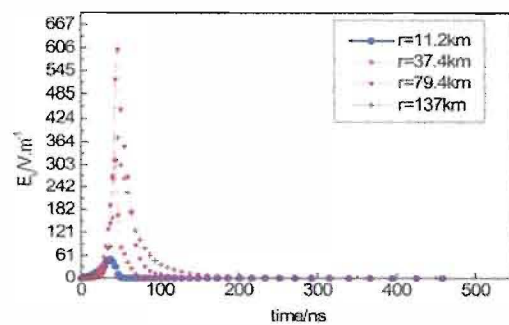


Fig. 11. Waveform of the electric field in the time domain, HOB is 20 km.

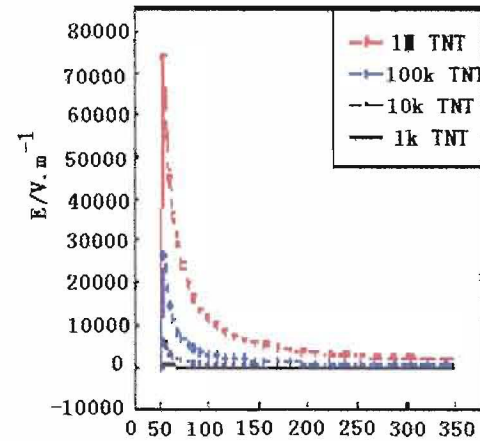


Fig. 12. HOB = 80 km, the waveform of electric field in the time domain at 150 km from the burst point.

too. Figs. 11 and 12 show the calculation results with different energies at explosion heights of 100 and 60 km. The power of the 100 kT explosion is 10 times less than that of the 1 MT nuclear explosion, with the electric field intensity peak down by 2.5 times; the power of 500 kT explosion is two times less than that of the 1 MT nuclear explosion, with the field intensity peak down by 15% only. As the power increases, the Compton-electron currents incited by the interaction of γ ray and air molecules grow, and the air conductivity increases too. Air conductivity is the damping term for electric field. They restrict each other to bring the electric field into the saturation area. Thus, the electric field intensity and energy will not change in a linear way.

Through calculations and analysis of the frequency range, with the effect of chromatic dispersion of the ionosphere considered, the low-frequency portion of source signals is reflected, and the high-frequency portion suffers chromatic dispersion by the ionosphere. Phases with high frequency have fast speed, those with low frequency have slow speed. The chromatically dispersed electric field becomes a damped oscillation waveform. In terms of the attenuation of amplitude, there is no change in the magnitude of peak values as compared with the former ones. The calculation resulted in the EMP field intensity at different explosion heights on the geosynchronous orbit when the total explosion energy is 1 MT (see Table II).

TABLE II
RELATIONSHIP BETWEEN THE ELECTRIC FIELD PEAK AND THE EXPLOSION HEIGHT FOR A SATELLITE ON GEOSYNCHRONOUS ORBIT (WITH YIELD OF 1 MT)

HOB (km)	Peak value of E-field, with distance of 150 km to the burst point (V/m)	Peak value of E-field, 36000 km Geosynchronous Orbit (V/m)
20	347.2	0.011
35	3926.0	0.114
40	4504.0	0.131
45	4764.5	0.138
50	4868.4	0.141
55	4835.0	0.140
60	4770.0	0.138
65	4512.5	0.130
70	4316.2	0.125
75	3966.6	0.115
80	3710.8	0.107
90	3000.0	0.087
100	2035.0	0.059

The numerical result is that after the 20–100 km nuclear explosion EMP is transmitted upward to the satellite orbit at 36 000 km, the field intensity peak of 1 MT TNT yield ranges from 10 to 100 mV/m; the field intensity peak of 1 kT yield ranges from 0.1 to 4 mV/m, and the background noise at this altitude is only 10 μ V/m; therefore, HEMP signals could be detected. Thus, nuclear explosions above 1 kT can be detected theoretically. The effect of yield on EMP peak values is less severe than that for explosion height variations. Also the relationship between the field intensity with the yield and HOB is nonlinear.

V. CONCLUSION

Through calculations, it is easy to find that the time waveform of HEMP looks like a double exponential waveform. The rise time is closely correlated to the rise time of γ rays. The HEMP is fast when the γ ray output is fast; on the path of downward transmission of the HEMP from the burst point, the lower it goes, the narrower the half width of the waveform; at a point on the ground closer to the explosion center, the narrower the half width of the time waveform. The half width in the deposition region is \sim 100 ns, while on the ground it is between 10 and 30 ns. Both in the deposition region and on the ground, the HEMP varies from 1000 to 80 000 V/m. With a fast rise time and a slow declining time, a HEMP waveform has abundant frequency spectra.

The numerical calculation result is that, after bursts between 20 and 100 km HOB, HEMP is transmitted upward to a satellite orbit at 36 000 km, and the peak value of electric field of 1 MT TNT yield ranges from 10 to 100 mV/m; the peak value of the electric field for a 1 kT TNT yield ranges from 0.1 to 4 mV/m, and the background noise there is only 10 μ V/m; therefore, HEMP signals could be detected. Thus, a nuclear explosion

above the magnitude of 1 kT can be detected theoretically. The effect of explosion yield on peak value is less severe than that of the explosion height. Also the relationship between the peak value of electric field with the power and explosion height are nonlinear.

ACKNOWLEDGMENT

The author acknowledges all the reviewers's suggestions. In particular, the author acknowledges Dr. Radasky, he modified the English of this paper and added technological explanation.

REFERENCES

- [1] W. Radasky, "The effects of three high power EM threats on electric power threats," presented at the Euro. Electromagn., Toulouse, France, Jul. 2012.
- [2] W. J. Karzas and R. Latter, "Satellite-based detection of the electromagnetic signal from low and intermediate altitude nuclear explosions," AD-61670I, Jun. 1965.
- [3] W. J. Karzas and R. Latter, "Detection of the electromagnetic radiation from nuclear explosions in space," *Phys. Rev.*, vol. 137, no. S8, pp. 1369–1378, 1965.
- [4] W. J. Karzas and R. Latter, "Electromagnetic radiation from a nuclear explosion in space," *Phys. Rev.*, vol. 126, no. 6, pp. 919–927, 1961.
- [5] T. C. Chapman, "A computer code for high altitude EMP," AD-777841, Jan. 1974.
- [6] T. Murphy, "Electromagnetic pulse (EMP) from surface burst," LA-11060-MS, Aug. 1987.
- [7] J. R. Lillis, "Theory of the high altitude electromagnetic pulse," AD-67418, Mar. 1974.
- [8] F. M. Tesche and P. R. Barnes, "Development of a new high altitude electromagnetic pulse (HEMP) environment and resulting overhead line responses," *IEEE Trans. EMC*, vol. 34, no. 6, pp. 93–99, May 1992.
- [9] C. L. Longmire and R. M. Hamilton, "A nominal set of high-altitude EMP environments," ORNL/Sub-86-18417/1, Feb. 1988.
- [10] C. Meng, "The numerical research of the effect of the transient electromagnetic field coupled to the multiple hole object," *High Power Laser Particle Beams*, vol. 12, no. 06, pp. 732–736, 2000.
- [11] C. Meng, "Numerical simulation of the early-time high altitude electromagnetic pulse," *Chin. Phys.*, vol. 12, no. 12, pp. 571–576, 2003.
- [12] C. Meng, "Effects of the HOB and the burst yield on the properties of NEMP," *Chin. J. Comput. Phys.*, vol. 20, no. 2, pp. 173–176, 2003.
- [13] C. Meng, "The analysis of the propagation of transient electromagnetic pulse through ionosphere," *Nuclear Electron. Detect. Technol.*, vol. 24, no. 4, pp. 369–374, 2004.
- [14] *Electromagnetic Compatibility (EMC) - Part 2: Environment - Section 9: Description of HEMP Environment - Radiated disturbance*, IEC 61000-2-9 Ed. 1.0, Feb. 1996.
- [15] C. L. Longmire, "On the electromagnetic pulse produced by nuclear explosions," *IEEE Trans. Electromagn. Compat.*, vol. 23, no. 6, pp. 1897–1902, 1976.
- [16] K. D. Leuthauser, "A complete EMP environment generated by high-altitude nuclear bursts," Theoretical Note 363, Oct. 1992. Available: <http://ace.unm.edu/summa/notes/TheoreticalPDFs/TN364.pdf>



Cui Meng (M'08) received the bachelor degree from Fudan University, Shanghai, China, in 1992 and the Doctor degree from Northwest Institute of Nuclear Technology, China, in 2003.

She did Postdoctoral Research in Tsinghua University, Beijing, China, during 2005–2007, and became an associate professor of Department of Engineering Physics, Tsinghua University, in 2007. Her current research interests include numerical simulating of high power electromagnetic environment, measurement of high power transient EMP.